



Review Paper

Fundamental study and utilization on supercritical CO₂ fracturing developing unconventional resources: Current status, challenge and future perspectives



Bing Yang^a, Hai-Zhu Wang^{a,*}, Gen-Sheng Li^a, Bin Wang^{a,b}, Liang Chang^c,
Gang-Hua Tian^a, Cheng-Ming Zhao^a, Yong Zheng^a

^a State Key Laboratory of Petroleum Resources and Prospecting, China University of Petroleum, Beijing, 102249, China

^b Craft Hawkins Department of Petroleum Engineering, Louisiana State University, Baton Rouge, LA, USA

^c Development Company of Xinjiang Oilfield, Karamay, 834000, Xinjiang, China

ARTICLE INFO

Article history:

Received 23 January 2022

Received in revised form

16 August 2022

Accepted 24 August 2022

Available online 30 August 2022

Edited by Yan-Hua Sun

Keywords:

Unconventional resources

Supercritical CO₂ fracturing

Experiment and numerical simulation

Fracture initiation and propagation

ABSTRACT

Under the fact that considerable exploration and production of unconventional resources and worsening global climate, reducing carbon emission and rationally utilizing carbon resources have been drawn increasing attention. Supercritical CO₂ (SC-CO₂) has been proposed as anhydrous fracturing fluid to develop unconventional reservoirs, since its advantages of reducing water consumption, reservoir contamination etc. Well understanding of SC-CO₂ fracturing mechanism and key influencing factors will exert significant impact on the application of this technology in the field. In this paper, the fundamental studies on SC-CO₂ fracturing from the aspects of laboratory experiment and simulation are reviewed. The fracturing experimental setups, fracture monitoring and characterizing methods, unconventional formation categories, numerical simulation approaches, fracturing mechanism and field application etc., are analyzed. The fundamental study results indicate that compared with conventional hydraulic fracturing, SC-CO₂ fracturing can reduce fracture initiation pressure and easily induce complex fracture networks with multiple branches. The field test further verifies the application prospect and the possibility of carbon storage. However, due to the limitation of reservoir complexity and attributes of SC-CO₂, massive challenges will be encountered in SC-CO₂ fracturing. According to the current research status, the limitations in basic research and field application are summarized, and the future development direction of this technology and relevant suggestions are proposed.

© 2022 The Authors. Publishing services by Elsevier B.V. on behalf of KeAi Communications Co. Ltd. This is an open access article under the CC BY-NC-ND license (<http://creativecommons.org/licenses/by-nc-nd/4.0/>).

1. Introduction

“Shale Revolution” has enabled the United States (US) to significantly increase its oil and gas production from tight reservoirs since the 21st century (Le, 2018). The success of the development of unconventional resources in US has drawn a lot of interest and attention to other countries in the world (Zhang et al., 2002; Yang et al., 2014; Lu et al., 2015; Zhang et al., 2019a). According to the statistics of the EIA and PetroChina, many countries such as China etc. (EIA, 2017; Sun et al., 2019), pose great potential and motives to replicate the Shale Revolution in US. These countries

expect to make breakthroughs in shale gas, tight gas, geothermal energy and coalbed methane, etc. (Kargbo et al., 2010; Tong et al., 2018; Jia et al., 2019; Sun et al., 2019). However, the geological conditions of a certain resource vary greatly from different reservoirs, which will lead to huge differences in terms of technologies and costs. Taking China as an example, compared with the conditions of shale gas reservoirs in North America, China's resources features are in deep formation depth, ultra-low permeability, complex geological stress condition, fragmented resources distribution, etc., all of which bring great challenges to exploration and development (Sun et al., 2019).

Currently, horizontal drilling and hydraulic fracturing are the commonly accepted methods to develop unconventional resources such as shale gas and tight oil, etc (Soliman et al., 2012). The most common fracturing fluid used for unconventional resources

* Corresponding author.

E-mail address: whz0001@126.com (H.-Z. Wang).

development is water-based working fluids. While significant success has been achieved in some fields, water-based working fluids present several obvious issues, including but are not limited to: 1) Since the existence of high content clay minerals in unconventional formation, water-based fracturing fluid can induce clay swelling, which will result in pore blocking and formation damage (Kargbo et al., 2010; Bazin et al., 2010; Bahrami et al., 2012); 2) Large-scale hydraulic fracturing consumes a large amount of water resources, but unconventional resources are mostly distributed in areas with complicate topography and water shortage, which brings huge challenges to field operations (Nicot and Scanlon, 2012; Scanlon et al., 2014; Wang et al., 2018); 3) Water-based fracturing fluids contain various toxic chemical additives, such as friction reducers, thickening agents, gelling agents, crosslinkers, swelling inhibitors etc., which can cause significant pollution to groundwater and surface environment, also increase the treatment cost for flowback fluid (Osborn et al., 2011; Gregory et al., 2011; Jackson, 2013; Lenhard et al., 2018). To address these issues, researchers are seeking alternative anhydrous fracturing fluid. CO₂ has been proposed as a particular working fluid for developing unconventional resources (Middleton et al., 2015). By injecting CO₂ into subsurface for fracturing, it not only can reduce carbon emission, but also is capable of enhancing hydrocarbon recovery (Solomon et al., 2009; Song et al., 2021; Guo et al., 2020, 2022). Using CO₂ as fracturing fluid shows great potential to mitigate the global climate and promote sustainable development of energy (Faruque Hasan et al., 2014; Wang et al., 2014; Edwards and Celia, 2018, Zhang et al., 2019b).

Studies show that when formation depth is greater than 1000 m, the temperature and pressure will exceed the critical point of CO₂ (31.1 °C, 7.38 MPa, respectively), thus CO₂ will reach the supercritical state at this subsurface condition. Supercritical CO₂ (SC-CO₂) has many unique properties, such as low viscosity, strong diffusion, much higher density than gas, and almost no surface tension, etc. (Espinoza and Santamarina, 2010; Wang et al., 2012). Many studies indicate that SC-CO₂ is able to avoid the clay swelling in unconventional reservoir (Pei et al., 2015), enhance natural gas recovery by displacing adsorbed methane (Zhou et al., 2018). In addition, SC-CO₂ is almost pollution-free to surface environment and poses no threat on water resource (Middleton et al., 2014, 2015). For these reasons, SC-CO₂ is considered as a promising fracturing fluid to exploit unconventional reservoirs.

This paper is to review the state-of-the-art fundamental research and related application on SC-CO₂ as fracturing fluid, including laboratory experiments, numerical researches. And the principal findings for fracture initiation and propagation is summarized through these studies. Then, representative field trials are discussed. Eventually, the problems existing in current research are analyzed and some recommendations are given for future research.

2. The methods of experimental and numerical study of supercritical CO₂ fracturing

In this section, the laboratory experiments and numerical simulation studies of SC-CO₂ fracturing are reviewed. The experimental methods, reservoir types, fracture analysis methods, and relevant results obtained from these experiments are summarized. Then, the simulation methods and corresponding simulation results with respect to SC-CO₂ fracturing are analyzed. The fracture initiation mechanism, fracture propagation characteristics and advantages of this method compared with conventional fracturing methods are concluded, also the problems existing in the current researches are discussed.

2.1. Laboratory study of fracture initiation and propagation with supercritical CO₂ fracturing

2.1.1. Experimental setup

To conduct SC-CO₂ fracturing experiments, a comprehensive laboratory system needs to be developed. Since the supercritical state of CO₂ is under reservoir conditions of pressures (>7.38 MPa) and temperature (>31.1 °C), an experimental device that can achieve reservoir conditions should be designed to perform fracturing experiments. Compared to the conventional fracturing experimental setup, a special fluid generation and pumping system is required for SC-CO₂ fracturing experiments. The CO₂ is initially stored as a liquid state, then is heated and pressurized to turn it into a supercritical state, and finally a rock sample is fractured in the stress-applied system. Additionally, the fracture initiation and propagation process is monitored and quantified by different approaches. In summary, the whole experimental system can be divided into the following units: a CO₂ pumping system, a tri-axial loading system, a core holder unit, a temperature-control unit and control/measurement system etc. According to the different experimental stress conditions, the fracturing system is divided into pseudo-triaxial and true-triaxial fracturing devices (as shown in Fig. 1 and Fig. 2).

- (1) Fracturing experimental system based on pseudo-triaxial stress.

To simulate the natural stress regime under subsurface formation, a widely used fracturing system on the basis of pseudo-triaxial stress condition is proposed. As shown in Fig. 1, this triaxial fracturing system is usually composed of a fluid-injection pump, a triaxial-stress loading system, a core holder unit, a temperature-control unit (water-bath system), a control/measurement system, etc. The fracturing system is loading with a cylindrical rock sample (As depicted in Fig. 3a), which can simulate vertical and horizontal principal stress conditions in subsurface formation by applying various axial and radial pressure to the rock sample. Considering that fracturing experiments are performed on cylindrical rock samples, there are three stress conditions can be applied: 1) triaxial compression test, where the minimum and maximum horizontal stresses are equal and applied as the confining stress, which is less than the axial stress ($\sigma_c < \sigma_a$). 2) triaxial extension test, where the confining stress is greater than the axial stress ($\sigma_a < \sigma_c$). 3) hydrostatic test, where the confining and axial stresses are equal (that is, $\sigma_a = \sigma_c$) (Zoback, 2010). Since it can simulate various formation stress conditions and support a wide range of sample dimensions (diameter of 25–100 mm and length of 50–200 mm), this experimental system is widely utilized in fracturing experiments (Bennour et al., 2015; Li et al., 2016; Zhou et al., 2016; Hou et al., 2017; Zhao et al., 2018; Zhang et al., 2020; Yang et al., 2021a; Zhang et al., 2022). However, since there is no difference in horizontal principal stresses, it is not consistent with the actual formation stress condition. Therefore, a true triaxial fracturing system that can realistically simulate formation stress conditions is proposed to investigate fracturing processes, which will be introduced in next section.

- (2) Fracturing experimental system based on true-triaxial stress.

To solve drawbacks in the pseudo-fracturing experimental system, a SC-CO₂ fracturing system under true triaxial conditions is proposed. Different from pseudo-triaxial stress system, this stress system is modified into a cube shape. It can be seen from Fig. 2 that this fracturing system can be used to simulate horizontal stress differences and explore the effect of true stress conditions on

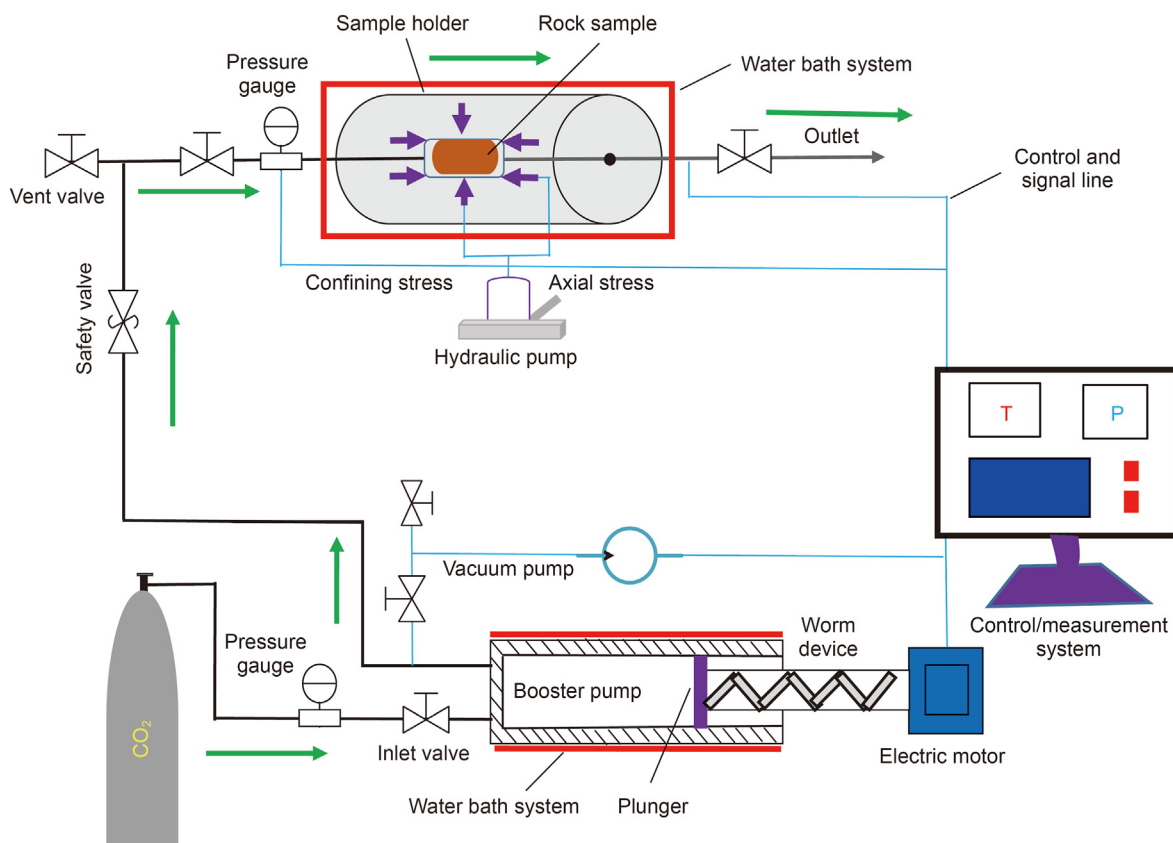


Fig. 1. SC-CO₂ fracturing experimental system based on pseudo-triaxial stress (Yang et al., 2021a, b).

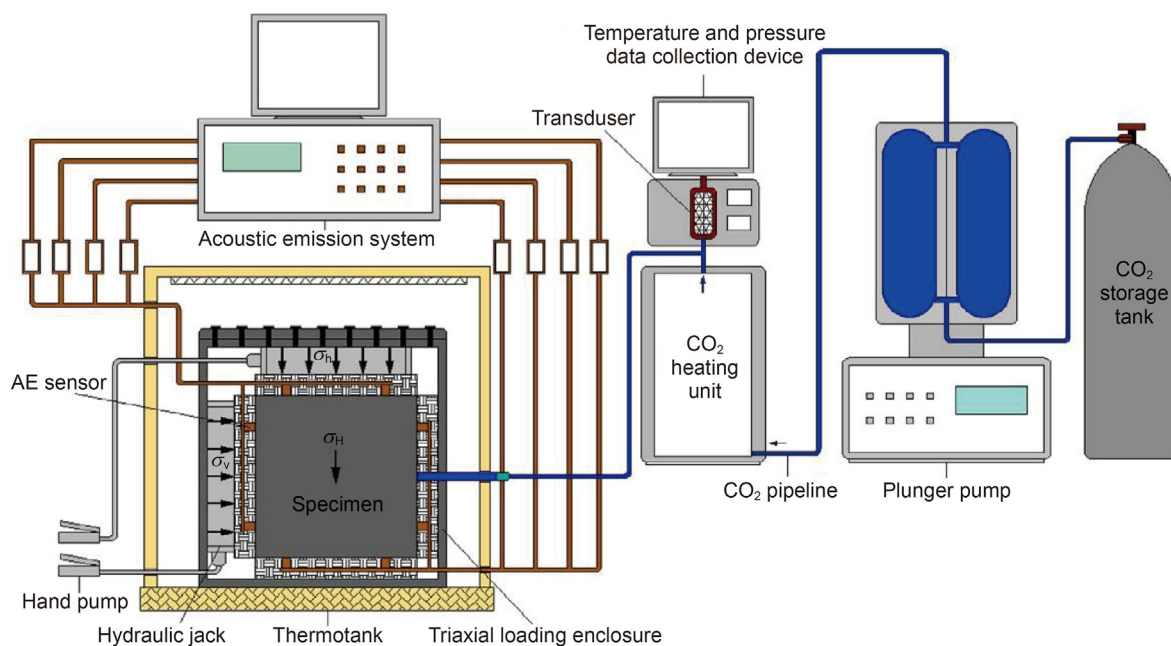


Fig. 2. SC-CO₂ fracturing experimental system based on true-triaxial stress (Zhang et al., 2017a).

fracture initiation and propagation. This allows fracturing experiment is consistent with field test results. Moreover, the system supports a much larger sample sizes (edge length of 100–1000 mm) compare to pseudo-triaxial system. A schematic of rock is shown in Fig. 3b (Ishida et al., 2004, 2012; Zhang et al.,

2017a, 2022; Wang et al., 2017b; Zhou et al., 2018a; Zou et al., 2018; Li et al., 2019; Hu et al., 2019).

However, considering the rigorous requirements on experimental conditions of SC-CO₂ and the stress loading tool is non-transparent metal mould, neither of the above experimental

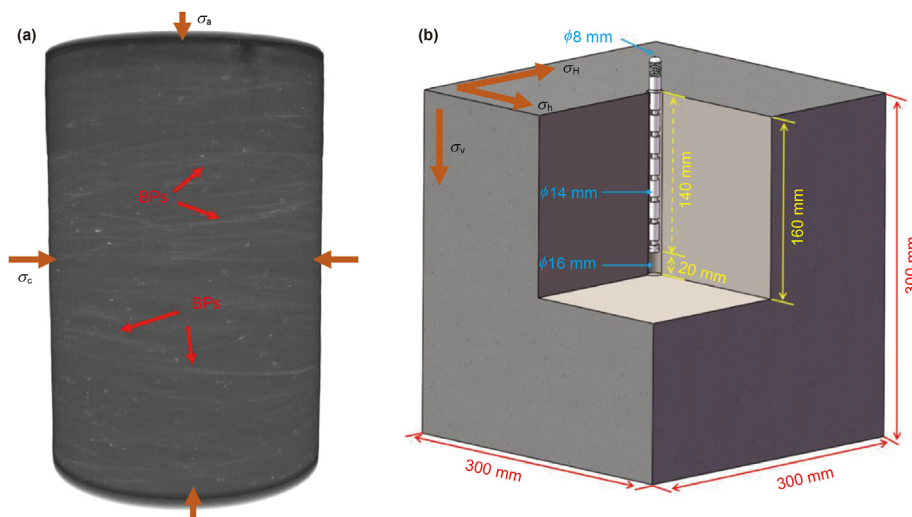


Fig. 3. Schematics of rock shapes for (a) pseudo-triaxial stress system (Bennour et al., 2015; Zhou et al., 2016; Yang et al., 2021a, b) and (b) true-triaxial stress system (Zhang et al., 2017a; Zhou et al., 2018a).

systems can directly observe fracture initiation and propagation in real time. Under the limitation of this issue, scholars attempt to explore a visual fracturing experimental system that can realize real-time monitoring (Gonçalves da Silva and Einstein, 2018; Amarasinghe et al., 2020). Some scholars use high-speed photography to monitor the fracturing process by removing stress-loading molds in some stress directions, also replacing rock sample with transparent materials (Alpern et al., 2012; Zhou et al., 2018b). Although, this method can directly observe fracturing process, it is hard to achieve the triaxial stress conditions. And, the properties of transparent materials, such as polymethyl methacrylate (PMMA), are quite different from real formation, which cannot be completely regarded as fracturing process of the reservoir.

2.1.2. Formation types

As mentioned in Section 1, SC-CO₂ used as fracturing fluid is aimed to exploit unconventional reservoirs such as shale gas, tight oil and gas, coal bed methane, geothermal resource, etc. Therefore, fracturing experiment studies are principally focus on formation with respect to shale, tight sandstone, coal, granite and certain artificial materials like cement stone and PMMA, etc. This section, we will review rock types used in fracturing experiments, and describe related research purpose.

As shown in Fig. 4 and Table S1 in Supplement Material, a large number of fracturing experimental studies of shale are conducted (Bennour et al., 2015; Li et al., 2016; Zhao et al., 2018; Zhang et al., 2017a; Zhang et al. 2020; Jia et al., 2018; Wang et al., 2017b; Jiang et al., 2018; Deng et al., 2018; He et al., 2019; Zhang et al., 2019a, b; Ranjith et al., 2019; Shafloot et al., 2021). These studies are focused on understanding CO₂ fracturing initiation, propagation, fracture characteristics and other aspects. It provides critical theoretical fundamentals for field application, and greatly promotes the application of CO₂ fracturing for the development of shale gas reservoir. In addition, while CO₂ is injected into subsurface to enhance oil and gas recovery, the potential of carbon storage in shale is also being explored (Abedini and Torabi, 2014; Lashgari et al., 2019).

Other unconventional resources, such as tight gas, coalbed methane etc., are also widely distributed around the world (EIA, 2017; Sun et al., 2019; Hou et al., 2015; Zheng et al., 2018). As mentioned in the section of introduction, CO₂ is a promising working fluid for fracturing especially for unconventional

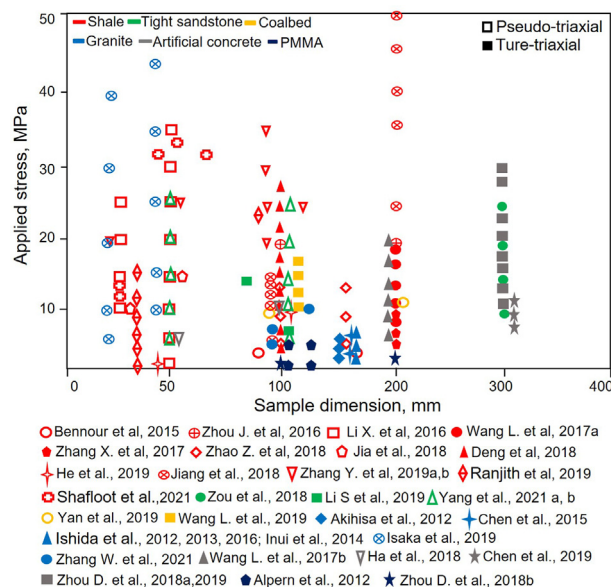


Fig. 4. Statistics on SC-CO₂ fracturing experimental research in the literature (Bennour et al., 2015; Li et al., 2016; Zhou et al., 2016; Zhao et al., 2018; Yang et al., 2021a, b; Ishida et al., 2012, 2013; Zhang et al., 2017a; Jia, YZ et al., 2018; Jiang et al., 2018; He et al., 2019; Zhang et al., 2019a, b; Ranjith et al., 2019).

resources. Numerous studies have been conducted on CO₂ fracturing in these reservoirs as well (Zou et al., 2018; Li et al., 2019; Yan et al., 2019a; Wang and Liang, 2019; Yang et al., 2021a, b). Fig. 4 shows the rock sample parameters for tight sandstone and coal rock in detail.

Also, in the context of global warming, renewable geothermal energy plays an important role to reduce carbon emission. Though water-based hydraulic fracturing has been widely used as the stimulation method in EGS project, the use of water for fracturing in EGS will also faces several issues, including environmental contamination, water shortage, formation damage, etc. (Breede et al., 2013). Thus, CO₂ was considered as the circulation fluid of EGS in 2000, and it shows several advantages for heat extraction from hot dry rocks (Brown, 2000; Pruess, 2008). Moreover, as CO₂ will continuously leaked and trapped in the formation rock during

the circulation process, using CO₂ in EGS can also serve the purpose of CO₂ sequestration. It provides the auxiliary benefit of earning credits for reducing greenhouse gases (Randolph and Saar, 2011). To successfully introduce SC-CO₂ as a fracturing fluid in EGS, researches on SC-CO₂ fracturing granite under high temperature are performed recently (as seen from Fig. 4 and Table S1 in Supplementary Material) (Ishida et al., 2012, 2013, 2016, 2017; Inui et al., 2014; Chen et al., 2015; Isaka et al., 2019; Zhang et al., 2021).

It is obvious that fracturing studies based on real rock samples is relevant to realistic reservoir condition, but it is challenging to observe and quantify the internal structure and fracture characteristics in a non-intrusive manner based on real rock sample. To investigate internal temperature field and the influence of perforation angle on fracture propagation during CO₂ fracturing, artificial cement specimens were adopted to replace rock samples for installing sensors and different perforating tools inside (Zhou et al., 2018a, 2019; Wang et al., 2017a; Ha et al., 2018; Chen et al., 2019). Also, for observing the process of fracture initiation in real time, transparent materials, such as PMMA, are manufactured to substitute intact rocks. The mechanism of fracture initiation and propagation was studied by recording the whole process with high-speed camera (Zhou et al., 2018b; Alpern et al., 2012). However, while synthetic materials bring convenience and observability for experimental investigation, the experimental results are difficult to be extended to field applications because of the huge differences in synthetic materials and reservoir rocks. For example, heterogeneity, bedding planes and natural fractures from real rock sample is known that has significant influence on fracture initiation and propagation.

2.1.3. Fracture monitoring and analysis approaches

The purpose of fracturing experiment is to characterize the fracture morphology and reveal the fracture initiation and propagation mechanism. Monitoring the process of fracture developments is one of the most important yet challenging procedure in experiments. Over the last several decades, many monitor tools, techniques and related algorithms have been used to qualitatively or quantitatively analyze fracture attributes in SC-CO₂ fracturing experiments. In this section, monitoring and analysis approaches will be reviewed, including manual optical measurement, acoustic emission (AE) monitor, profilometry, 2D slice scan, 3D CT scan, etc.

(1) Manual optical observation method.

Manual optical observation is the most common method for measuring fracture distribution and obtaining fracture propagation modes (Jia et al., 2018), fracture width (Wang et al., 2017b; Zou et al., 2018) and spatial distribution (Li et al., 2019), etc. This method is used to obtain fracture morphology by directly observing fractured rock or by labeled with dying solution, a comparison of different fracture analysis methods is shown in Table 1. The width distributions of fractures are measured artificially with rulers along the fracture extension on rock surfaces (as shown in Fig. 5). Moreover, the spatial shapes of fractures are manually reconstructed according to the labeled location on external and internal fracturing surfaces. The geometric parameters of fractures and complexity of fracture are characterized qualitatively (Zhou et al., 2018a; Zhang et al., 2019a; Chen et al., 2019). This method is widely used by researchers since it is straight-forward to perform, and applies for rock sample with a wide range of sizes (mostly adopted for large rock sample). However, this method is often limited for the case of characterizing fractures on the external surface of a rock sample, or observing internal fractures after rock sample is artificially broken. When we breaking the fractured rock sample with external forces, it may introduce lots of secondary

fractures that are not originally induced from fluid injection. Thus, it is an intrusive and quantitative method for fracture analysis.

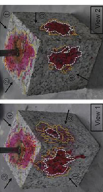
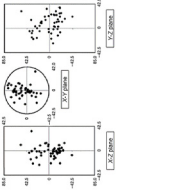
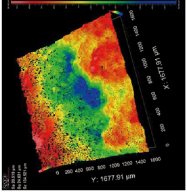

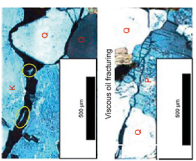
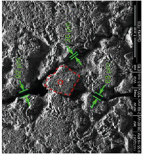
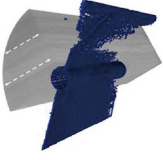
(2) AE monitoring in fracturing process

AE monitoring is another popular fracture characterization method. It is an indirect detection method to determine the progress of fracture generation by monitoring changes in acoustic signals induced from fracturing events (the characteristics of this method are shown in Table 1). In recent years, it has been commonly used in fracturing experiments to study fracture propagation mechanisms (Ishida et al., 2012, 2013, 2017, 2021). The AE monitoring system consists of sensors, pre-amplifiers, signal conditioner, A/D converter, memorizer, etc. Received AE signals are firstly amplified by preamplifier and a signal conditioner, and then recorded on a hard disk through an A/D converter (Ishida et al., 2012; Hamstad, 1986). When rock failure occurred, elastic waves are consequently emitted and propagated outward. The recording of an AE event is triggered when the signals exceeds certain threshold value of AE sensors. Due to the different patterns of AE events, the AE counts and amplitude in each sub-stage is significantly distinct (Li et al., 2018, 2019). AE monitoring can provide valuable information, including the spatial localization, hypocenter mechanism, AE amplitude, etc. Through AE signal, the initiation time and location of fractures can be obtained, and the failure mode of specimen can be analyzed as well (as shown in Fig. 6. When the compressional or dilatational motions dominate the signals, the corresponding AE events are named as tensile and compressive events, respectively; otherwise, they are named as shear events. So mechanical failure modes could be statistically estimated in terms of the proportion (λ) of dilatational first motions in all well-identified P-wave polarities (Lei et al., 1992; Zang et al., 1998). The effects of fluid on distribution of AE sources and fracture modes are discussed by Inui et al. (2014). And statistical analysis of the P wave polarity of AE waveforms indicated that the AE events associated with the SC-CO₂ induced fractures were dominated by shear failure (Ishida et al., 2012, 2013; Bennour et al., 2015; Zhang et al., 2017a; Zou et al., 2018). Furthermore, fractal dimensions of the distributions of the located sources can be obtained by the correlation function method (Lei et al., 1992). A larger fractal dimension indicates that locations of AE sources are more likely to distribute in three dimensions rather than along a flat plane, suggesting the induced fracture extending in a three-dimensional manner (Ishida et al., 2012; Hirata et al., 1987). However, this method is sensitive to external environmental noise signals. To obtain a valid data from experiments, sophisticated post-processing algorithms, such as denoising and artificial inversion are required.

(3) Optical microscope with fluorescent method

The geometric complexity of pore spaces and micro-fractures are frequently discussed in the hydraulic fracturing process. Aside from macroscopic definitions, the fluorescent method proposed by Nishiyama and Kusuda (1994) was applied to quantify microscopic fractures. Using image analysis method, their characteristics including porosity, and total length of micro-fractures per unit area, can be measured. The pore space and micro-fractures filled with resin and fluorescent paint can be observed and analyzed by microscopy on a polished rock surface under ultraviolet light (Bennour et al., 2015). It is straight-forward to observe morphology of micro-fractures and interactions between fractures and minerals. This technique can be used to obtain the microscopic fracture propagation patterns induced by different fluids. Previous research results concluded that a fluid with higher viscosity is more tended to result in a smoother fracture propagation path. While, injecting a

Table 1
Comparison of different fracture analysis methods (Modified from Yang et al., 2021a).

Approach	Manual imaging	AE	Profilometry	3D scanner	Optical micrograph	Electric micrograph	CT
Description							
View dimension	3D	3D	3D	3D	2D	2D	2D/3D
View filed	Local/whole	Whole	Local	Local	Local	Local	Whole
View size	5–30 cm	5–30 cm	20/100 mm				
Quantitatively	Poor	Good	Good	Good	Good	Good	Good
Intrusiveness	Strong	Weak	Strong	Strong	Strong	Weak	Weak
Accuracy	Low	Medium	High	High	Medium	High	High
Simulation	Hard	Hard	Yes	Yes	Hard	Hard	Yes
model							
Reference	Zou et al. 2018; Wang et al., 2017a, b; Wang and Liang 2019	Ishida et al. 2012; Zhou et al., 2017a; jia et al., 2018a	Li et al. 2016; Zhang X. et al., 2017a; jia et al., 2018	Zhao et al. 2018; Zhang Bennour et al., 2015; Li et al., 2019; He et al., 2019; Ranjith et al., 2019	Jia et al. 2018	Li et al., 2019; He et al., 2019; Ranjith et al., 2019	Isaka et al. 2019; Yang et al., 2021a; Shafiq et al., 2021

lower viscosity fracturing fluid causes intermittent and stepwise fracture propagation path (Ishida et al., 2016). Recently, microscopy is performed on the shale, concrete etc., which fractured by injection of fluid such as viscous oil, water, L-CO₂ and SC-CO₂. The microscopic observations of fractures are conducted and dyed minerals are recognized in Bennor's research. As depicted in Fig. 7, the fractures induced by low viscosity fluid such as SC-CO₂, are mainly propagated along the grain boundaries of the constituent minerals. Those specimens fractured by higher viscosity fluid, like water and oil, often cut through the mineral grains (Bennour et al., 2015; Chen et al., 2015; Ishida et al., 2016; Zhou et al., 2018a; Jia et al., 2018). However, the field of view for this method is typically less than few millimeters (as seen in Table 1), also the targeting area must be polished initially. These limitations prohibit this technique from being applied to relatively large rock samples.

(4) Electronic microscope technique

The scanning electron microscope (SEM), a versatile and useful tool for failure analysis. It has gradually replaced the transmission electron microscope (TEM) for fracture surface analysis since the early 1960's. This instrument is particularly useful in fracture analysis because (1) it supports a wide magnification of view, and (2) fractures can be viewed directly. With this instrument, one can determine the failure mode of a broken sample in a relatively short period of time. SEM is used in different magnifications to observe fractures at various length scale, pore structure, organic matter and inorganic morphologies of rock samples (Russo, 1978; Kanaori et al., 1991). In recent years, electronic microscope is employed by several researchers to get images of main fractures created by different fracturing fluids, which are obtained based on relatively lower magnifications (as illustrated in Fig. 8a) (Zhao et al., 2018; Deng et al., 2018; He et al., 2019). The geometric characteristics and curvature degrees (tortuosity) of main fractures are discussed. Also, fracture branches and their interactions with the main fracture can be analyzed. To observe micro-fractures in some regions of interest, higher magnifications could be used to obtain information about fracture width, surface topography of the surface and composition (as shown in Fig. 8b) (Li et al., 2019).

According to Li et al.'s results, CO₂-based fluids generate multiple fracture branches, many micro-fractures, and rugged fracture surfaces. However, water-based fluids would form a relatively smooth fracture surface with few micro-fractures and branches (Li et al., 2019). He et al. suggests that the micro-fractures can form the linkages between the organic pores, inorganic pores, minerals and organics (He et al., 2019). Similar to the optical microscope method, the scanning area of rock is usually limited to millimeter scale (as described in Table 1). Although this method can intuitively obtain accurate fracture characteristics, it brings difficulties to analyze full-size fractures. And the observed morphology is extremely sensitive to the selection of sample observation areas. By itself, the SEM cannot uncover all facts leading to the identification of the failure mechanism of a lab-scale rock sample (Diamond and Mindess, 1992).

(5) 3D profilometry and optical topography technique

The above two fracture observation methods even can intuitively obtain the plane characteristics and parameters (width, tortuosity, etc.) of microscopic fractures. However, most of these methods are significantly limited by size of field of view, and fracture characteristics are all analyzed in two-dimensional space. Therefore, 3D profilometry and optical microscopy testing are successively used to study the quantitative properties of fracture surfaces, including maximum, minimum value, root mean square

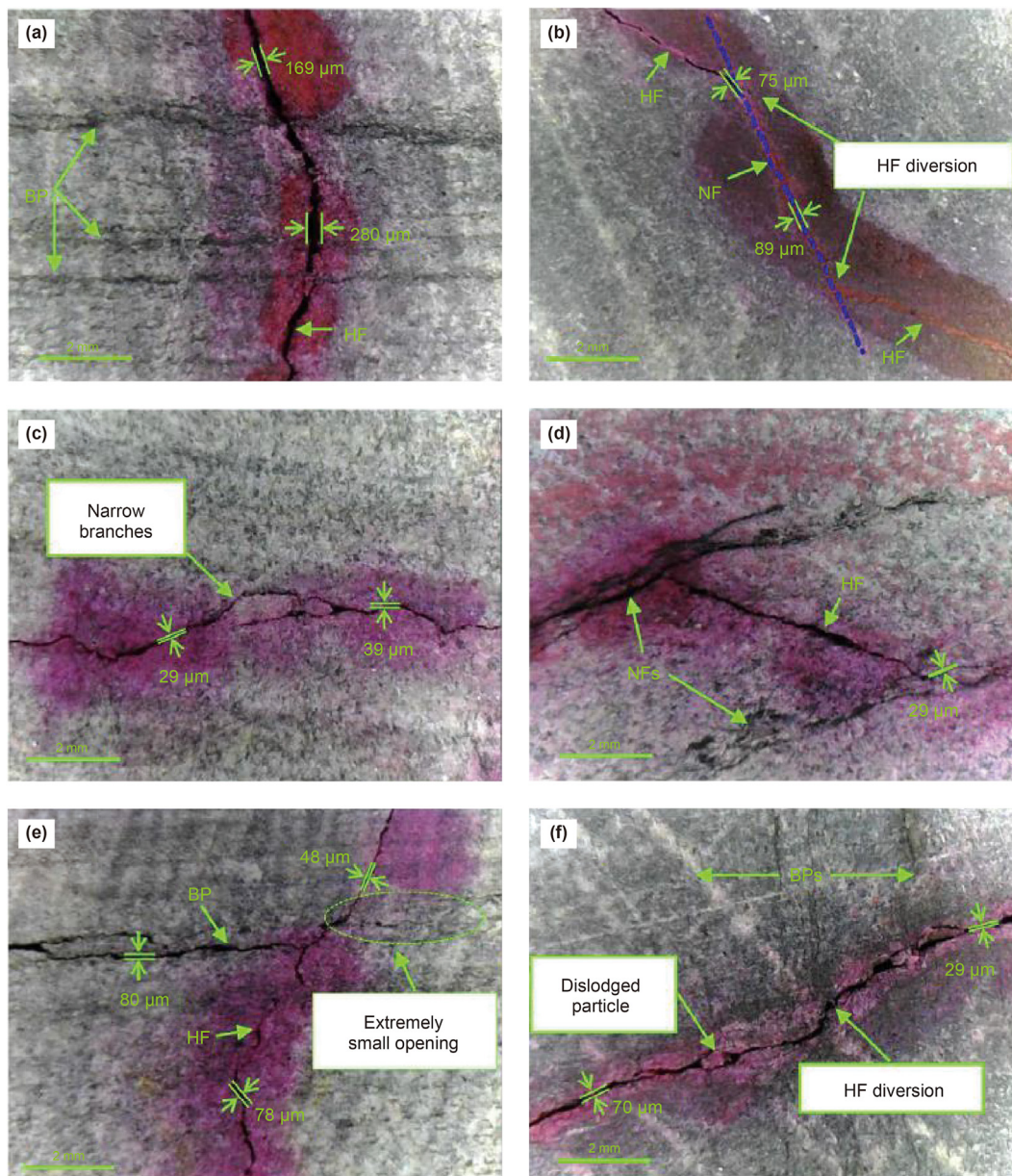


Fig. 5. Manual optical images of HF growth path at the local scale and fracture width created by different types of fluids: (a) x-linked guar, (b) slickwater, (c) to (f) SC-CO₂ (Zou et al., 2018).

(RMS) and standard difference of fracture aperture, fractal dimension and complexity, etc. According to the scanning methods, profilometry can be divided into stylus profilometry scan and optical profilometry. This technique was performed by Jia et al. (2018) and Li et al. (2019) to acquire the characteristics of 3D fracture surface, which can be seen from Fig. 9. Parameters of fractal dimension, fracture width and surface area ratio etc., were proposed to quantitatively evaluate fracture complexity, roughness and tortuosity in these studies (Li et al., 2016; Li et al., 2019).

Apart from the profilometry, another method to analyze the fracture surface is the 3D optical microscopy. After fracturing experiment, the fractured sample was then separated into two halves along the main fracture, and the fracture surface topographies were digitally imaged in XYZ point cloud format using a 3D optical topography scanner. Considering the arbitrary distance and angle between the scanner and the surface, a fitting plane of the

scanned surface was obtained based on the minimum deviation method (Zhang et al., 2019a). As shown in Fig. 10, three-dimensional scanner is used to get their morphologies and evaluate roughness of the fracture surfaces. The fractal dimension, height field, arithmetic mean and standard deviation of height field and area ratio (AR) are quantitatively characterized to describe the roughness of fracture surfaces (Zhao et al., 2018; Zhang et al., 2020). These two methods can realize 3D morphology and quantitative attribute analysis of fracture surface with a relative larger size of scanning region. However, the fractured rock sample must be manually broken into halves for scanning. The results are often affected by artificial intervention. Also, these parameters are usually obtained from regions of interest instead of whole fracture surfaces. Therefore, non-intrusive monitoring methods are needed to investigate the morphology of fracture surfaces.

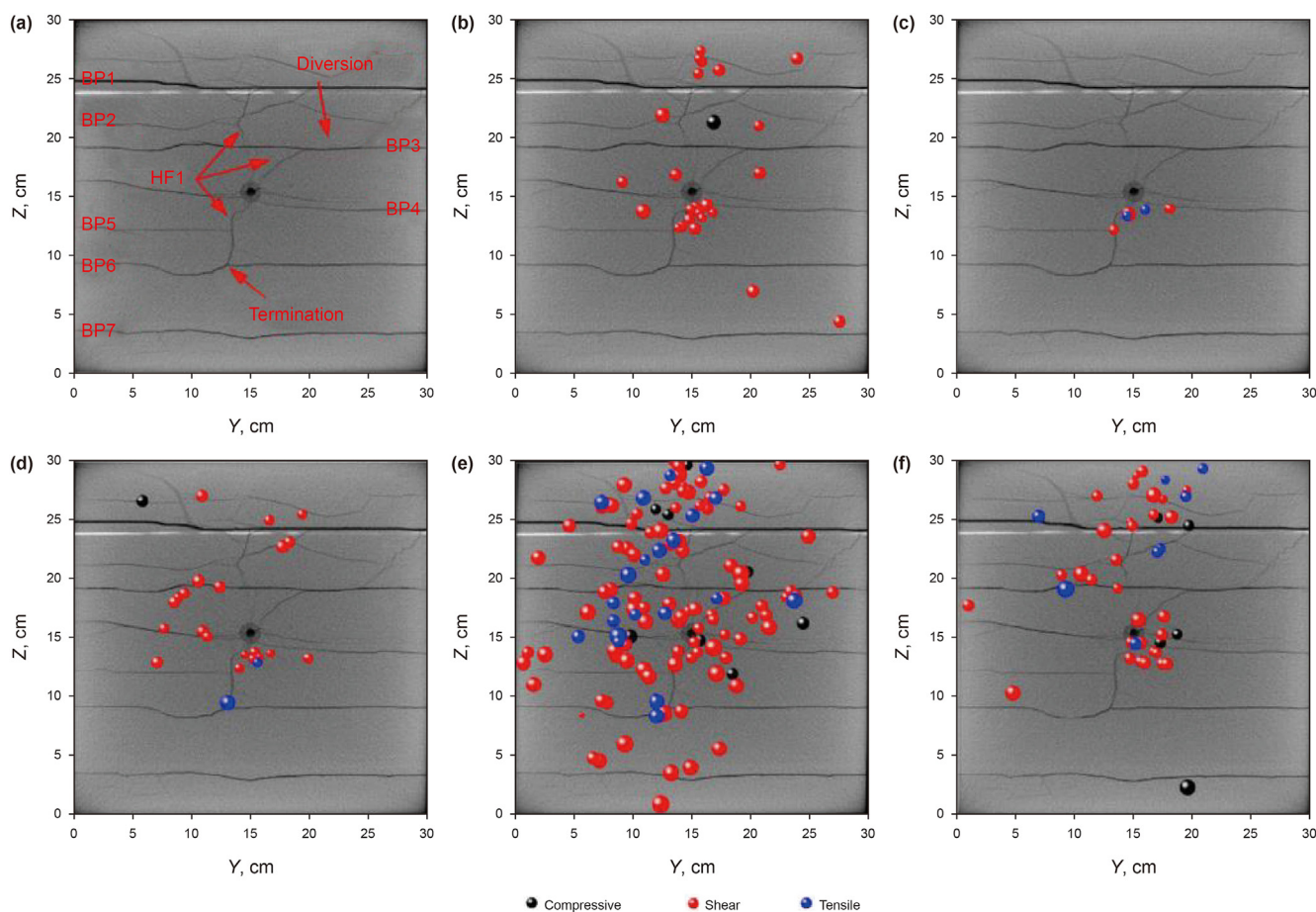


Fig. 6. Time dependency of the located AE events through the injection process of specimen (Li et al., 2018).

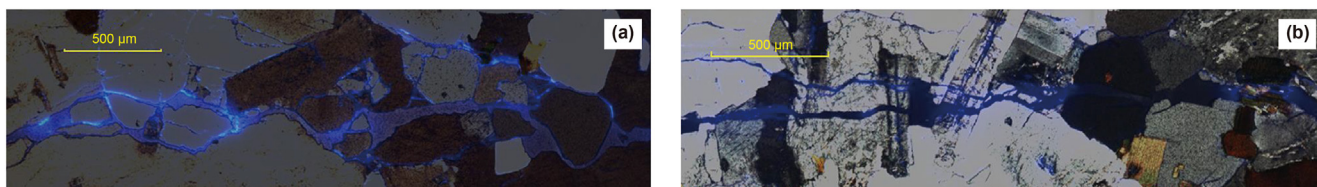


Fig. 7. Observations of the induced fractures and mineral grains by optical microscope with fluorescent method (Chen et al., 2015).

(6) Fracture analysis based on CT scanning.

CT scanning is able to identify internal fractures of rock without damaging the sample. It was utilized to visualize and quantify the generated fractures. Zhou et al. (2016), Zhang et al. (2017a), Zou et al. (2018) and Ranjith et al. (2019) implemented CT scanning to acquire 2D slice images of rock and to observe morphology and distribution of the induced fractures (Fig. 11). However, only a few slices of CT images in certain locations are scanned to represent whole fracture geometry. Also, no quantitative attributes of fractures are analyzed in these works.

Using 2D CT images, some researchers have reconstructed these into 3D samples based on image processing software, like Avizo, DragonFly etc. (Isaka et al., 2019; Jiang et al., 2019; Yang et al., 2021a, b). Three-dimensional reconstructions of CT scanning images are able to accurately characterize fracture morphology, fracture orientation, fracture spatial distributions and mineral composition. It can be found in Fig. 12 that Yang et al. (2021a), Ha

et al. (2018) and Shafloot et al. (2021) obtained the 3D fractures to quantitatively analyze the micro-morphology of fractures. The fracture network pattern, fractal dimension (FD), aperture, area ratio (AR) and fracture volume etc., are investigated. Compared with many conventional fracture analysis methods, this method can ensure the integrity of rock and avoid the generation of secondary fractures in the intrusive methods. Moreover, it can also avoid of using the local or some specific fracture attributes to represent the overall characteristics of whole fractures. However, because the X-ray intensity is significantly affected by the size of scanning objects, the size of rock samples is usually less than 100 mm (As listed in Table 1). Besides, there are also some limitations to identify and extract multi-scale fractures effectively. Therefore, it is necessary to improve CT scanning resolution and increase the scanning size in the future. Some algorithms for multi-scale fracture scanning and reconstruction are needed.

(7) Other characterization methods

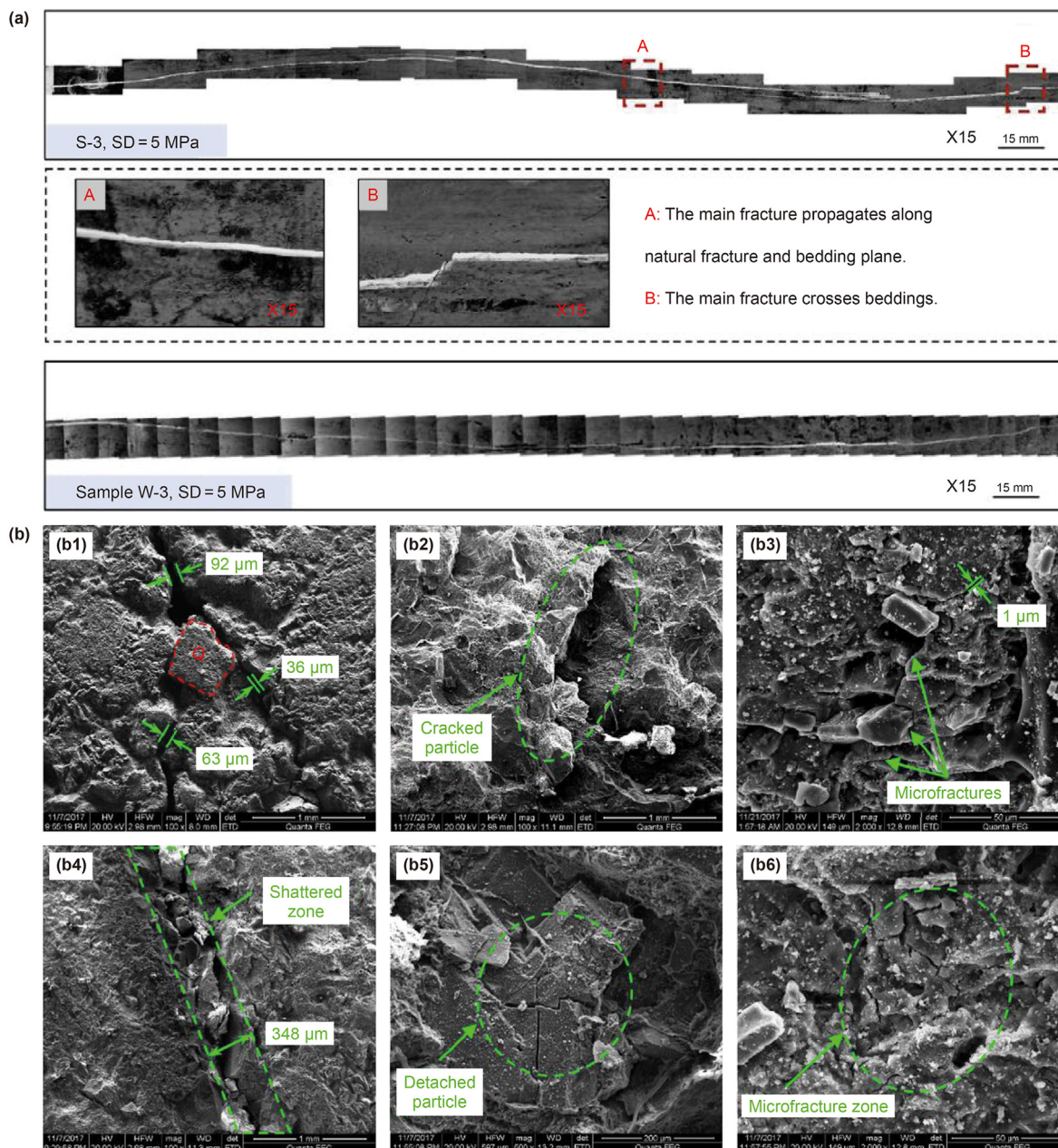


Fig. 8. Electronic microscope images of the micro-morphology of HFJs created by different fluid. (a) SC-CO₂ and water fracturing in shale (Zhao et al., 2018); (b) L-CO₂ and SC-CO₂ fracturing in tight sandstone (Li et al., 2019).

Besides fracture analysis approaches introduced above, the visual characterization methods are performed to monitor fracture propagation (Bhargava and Rehnström, 1975). Achieving real-time observations of fracturing process usually require the use of high-speed and high-resolution cameras. To explore the effect of SC-CO₂ phase transition on fracture dynamic propagation, high-speed camera was adopted to observe fracture development through a transparent PMMA sample by Zhou D. et al. (2018b). And the effect of the vertical loading and fracture geometries on the observed fracturing processes was investigated using a similar method by Gonçalves da Silva and Einstein (2018); Amarasinghe et al. (2020). Relying on real-time observation of fracture propagation, it will be a promising analysis method in the future. However, the synthetic transparent material typically has homogeneous mechanical properties and does not contain some representative features in

natural rocks, such as bedding planes, natural fractures and pore structure etc.

Recently, another popular method for real-time imaging of fracturing process is the digital image correlation (DIC) technique, which is an optical and a non-contact measurement method to visualize surface displacements (Skarzynski and Tejchman, 2013). The monitoring process is captured by tracking the deformation of a random speckle pattern applied to the surface through digital images acquired at different instances of deformation. Due to its availability, simplicity and low cost, this method is increasingly used in fracture mechanics analysis (Pan, 2018; Kan et al., 2018).

Also, for all these optical imaging methods, we cannot apply true triaxial stress conditions as an open side face is needed to set up the imaging system. Therefore, it is of great significance to explore a true triaxial fracturing system based on visualization in following study.

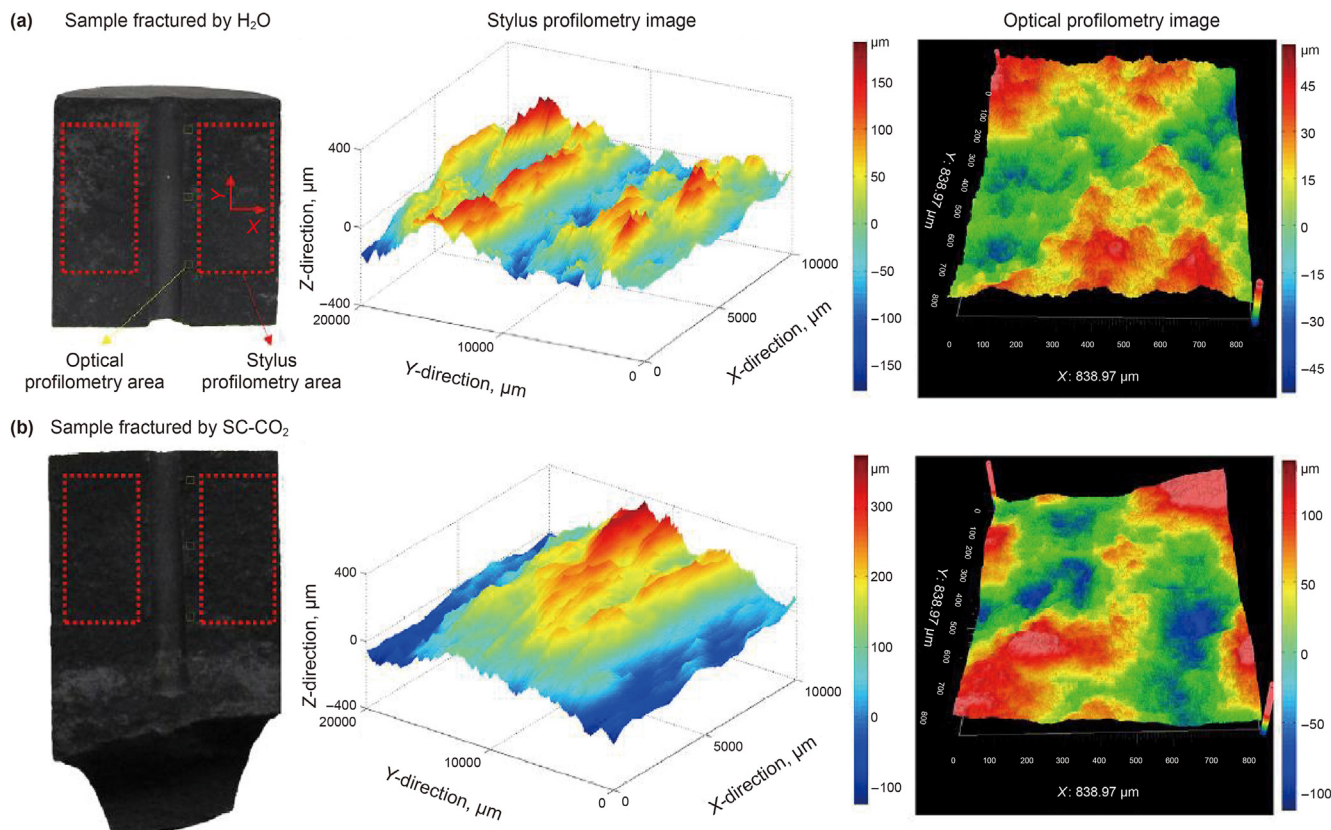


Fig. 9. Profilometry images for SC-CO₂ and H₂O fracturing. (a) Sample fractured by H₂O; (b) Sample fractured by SC-CO₂ (Li et al., 2016; Li et al., 2019; Jia et al., 2018).

2.2. Numerical simulation on SC-CO₂ fracturing

Due to the high cost of field operation and large-scale experiment, numerical simulation is the most economical and efficient way to simulate the process of drilling, well completion, and productivity forecast. Hydraulic fracturing modelling has been extensively studied in both petroleum engineering and fracture mechanics. In the recent decades, several numerical methods have been proposed and adapted to simulate hydraulic fracturing process, such as the finite element method (FEM), the extended finite element method (XFEM), the boundary element method (BEM), the discrete element method (DEM), Peridynamics theory, phase field method (PFM) etc. (Hattori et al., 2017). As one of the most popular numerical methods in fracture mechanics, FEM has long been adopted to simulate the propagation of hydraulic fracture (Advani and Lee, 1982; Boone and Ingraffea, 1990). Specifically, FEM is adopted to solve the rock deformation and fluid flow in reservoir. To further model the fracture-like failure, cohesive zone elements are then embedded into the model to simulate the fracture propagation (Carrier and Granet, 2012; Salimzadeh et al., 2017; Song et al., 2021). However, the highly refined meshing around the fracture tips are required when FEM was used for dynamic fracture propagation problems. To address this issue, extended/generalized finite element method (XFEM/GFEM) has also been proposed (Gupta and Duarte, 2014). Different from FEM, XFEM/GFEM captures crack discontinuity via discontinuous fields, namely the partition of unity functions. In the framework of XFEM, remeshing is circumvented by introducing the discontinuous fields but the computation of stress intensity factors is not as straightforward as that in FEM (Wang et al., 2017; Xu et al., 2017). However, XFEM/GFEM has the same limitation as standard FEM in terms of dealing with complex

topology produced from intersection between hydraulic fracture(s) and natural fractures, such as fracture branching and merging especially for 3D problems (Hattori et al., 2017; Roth et al., 2020).

The BEM is another popular modern approach for simulating both 2D and 3D hydraulic fracture propagation, including the presence of natural fractures. A fundamental difference between the BEM and standard FEM is that the discretization is applied only on the boundary of a domain (Cruse, 1968; Brebbia and Dominguez, 1977). Moreover, an indirect BEM formulation of displacement discontinuity method (DDM) is developed by Dong and de Pater (2001); Maso and Toader (2002) for hydraulic fracturing model. DDM is the most commonly used for problems with crack-like geometries. Compared with other continuum approaches such as FEM and XFEM, BEM is easier to implement with lower computational cost. Another advantage is that the mechanical behavior of natural fractures such as friction between opposite fracture surfaces are easy to be modeled in DDM formulation (Hattori et al., 2017; Chen et al., 2022). However, it is still hard to realize the simulation on intersection of arbitrary 3D hydraulic fractures in the scheme of BEM.

A non-continuum approach of discrete element method (DEM) model was first developed by Cundall (1971) to analyze rock mechanics problems. Different from the continuum approach, this model describes the rock media as a discrete system of deformable polygonal blocks. No extra fracture criterion is needed in this approach to model the fracture propagation. And there is no need to update the topology with the propagation of hydraulic fracture (Qu et al., 2020). However, a major drawback of DEM is its computational cost. Large particles or blocks are needed to make the simulation of field-scale problems affordable. Another one is that the stimulated fracture network is presented by discrete

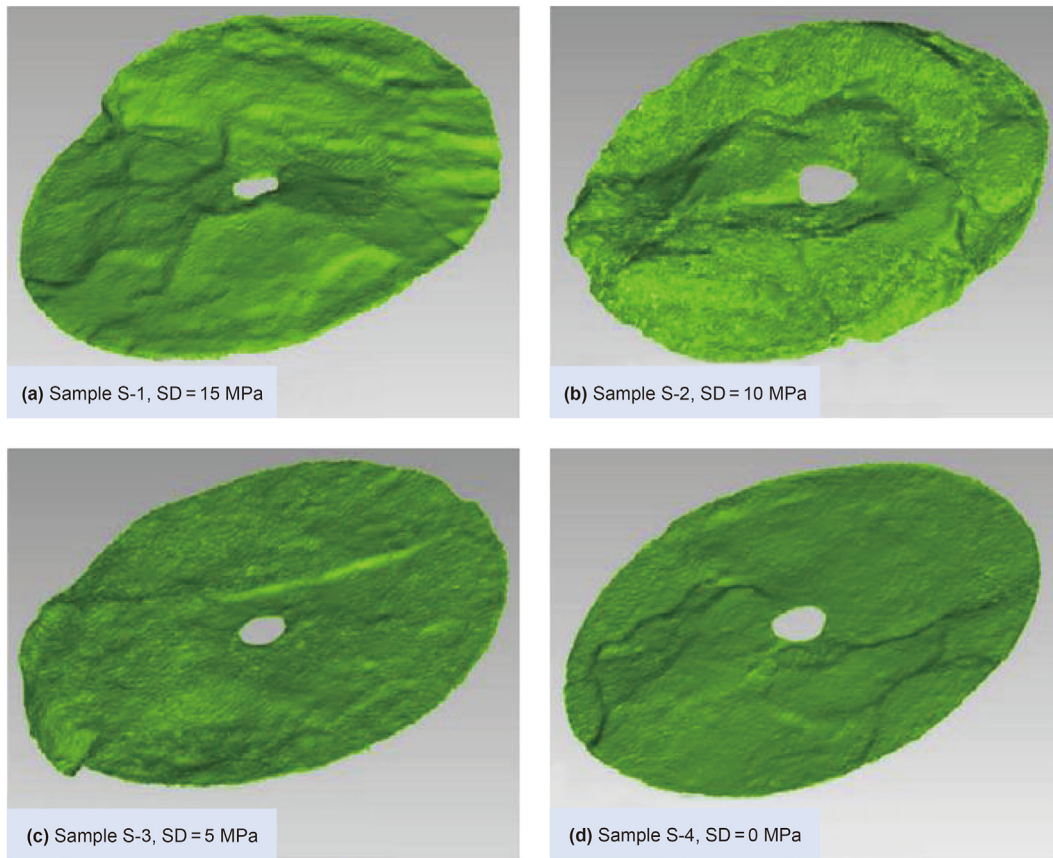


Fig. 10. Reconstructed main fracture surfaces by three-dimensional scanner (Zhao et al., 2018; Zhang Y. et al., 2019a).

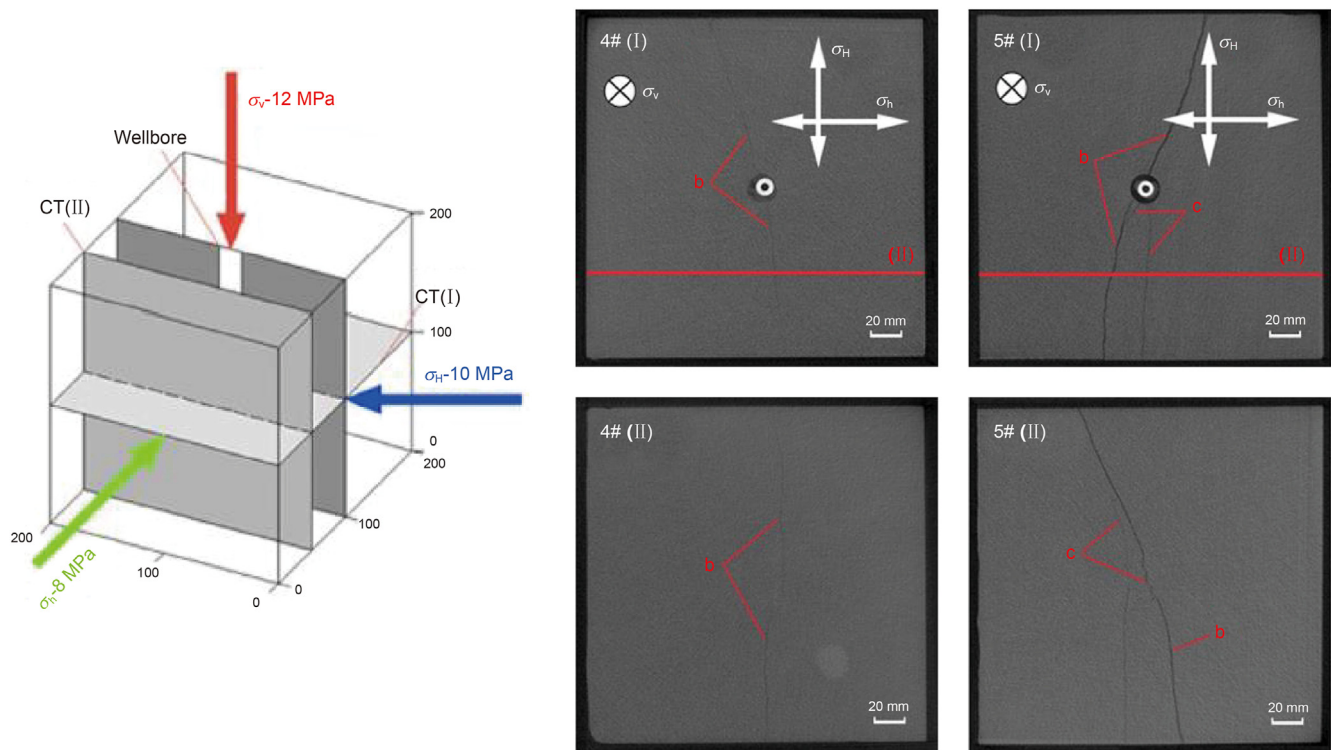


Fig. 11. CT scanning images of sandstone specimens. Specimen 4# was fractured with water, specimen 5# with SC-CO₂ (Zhou et al., 2016; Zhang et al., 2017a)

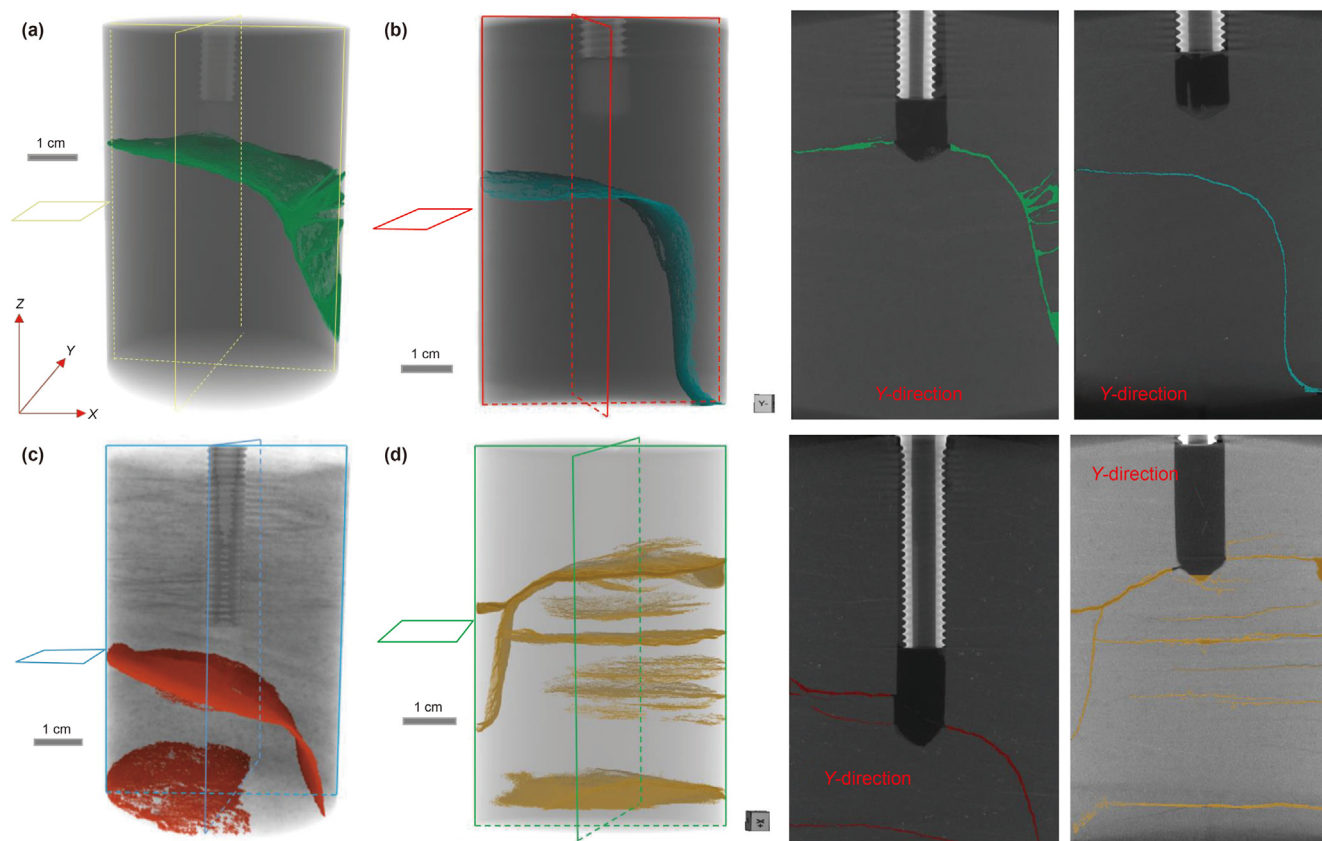


Fig. 12. The 3D fracture reconstruction profile induced by different fluids based on CT scanning. (a) Water-based fracturing; (b) N_2 -based fracturing; (c) L - CO_2 -based fracturing; (d) SC - CO_2 -based fracturing) (Yang et al., 2021a).

particles, which is not consistent with the real fracture shape. The description of fracture width is also not straight-forward based on this representation (Wang et al., 2018c).

The Peridynamics theory is proposed to represent a material as a composition of material points, each of which interacts with the other material points inside a horizon. The interaction between the material points is related to the deformation and constitutive properties of the material (Silling, 2000). As a non-local continuum mechanics approach, Peridynamics method is mesh free, which makes it easier to model complex fracture networks. Also, with a relatively easy crack propagation criterion, the fracture initiation and propagation can be captured spontaneously without complicated computations.

As a mathematically rigorous framework to solve interface problems, phase-field method has been applied in many areas including solidification dynamics, coarsening and grain growth, multiphase flow, microstructure evolution, fracture mechanics (Pilipenko et al., 2011; Mikelic et al., 2015; Hattori et al., 2017). The development of the PFM provided an alternative formulation when dealing with different interface problems. PFM treats the fracture propagation together with the deformation of surrounding medium as an energy minimization problem according to the minimum total potential energy principle (Lepillier et al., 2020). The PFM approach has been widely used recently since its several advantages: (1) there is no need to represent the discrete fracture surfaces by remeshing, which makes it possible to simulate the complex intersection of hydraulic and natural fractures especially in 3D space; (2) no extra fracture propagation criterion is needed since Griffith's criterion has been recast into the bulk energy functional; and (3) media heterogeneity is easy to be introduced

into the solution scheme (Chen et al., 2022). However, the method of PFM is high in computational cost, especially when a relatively sharp interface embedded in a model.

The numerical methods mentioned above have been developed for conventional hydraulic fracturing simulation. However, these methods are mostly based on incompressible water-based fluids. In the case of compressible CO_2 -based fluid, since its properties significantly change with temperature and pressure, the fracturing mechanism is also different from traditional fracturing process. In this section, we draw an outline of hydraulic fracturing simulation with SC - CO_2 . The status and development tendency of main numerical method on SC - CO_2 fracturing will be discussed.

From the current research reports, there are few of numerical studies with respect on SC - CO_2 fracturing. According to the numerical research on CO_2 fracturing listed in Table S2 in Supplementary Materials, the research method on fracture initiation and propagation are mainly divided into four types: (1) fracturing simulation based on FEM-based algorithm; (2) XFEM; (3) PFM; and (4) DDM. Initially, FEM algorithm combined with partial secondary development or mechanic theory is the most popular method to simulate CO_2 fracturing process. Zhang et al. (2017b), Zhang et al. (2019c), and Wang et al. (2018b) proposed numerical model based on this method to comparatively investigate the impact of viscous oil, water, nitrogen and CO_2 as fracturing fluids on fracturing mechanism. The concept of FEM-based damage mechanics, that combine the maximum tensile stress theory and the Mohr-Coulomb theory, was introduced together by Liu et al. (2018) to predict fracture propagation behavior in heterogeneous rocks. In the coupled models, rock damage, anisotropy of formation and fluid properties for both slightly compressible (water and oil) and

compressible fluids (CO₂, N₂) are considered under isothermal condition. The impacts of rock heterogeneity, Biot's coefficient, confining pressure, interfacial tension and fracturing fluid type on the fracturing process are investigated as well (the effect of orthogonal joint is shown in Fig. 13). Afterwards, Zhang et al. (2021) embedded MATLAB script into FEM software of COMSOL to achieve efficient solution of the established THMD coupling model. Then a three-dimensional fracture propagation process of hot dry rock fracturing under thermal stress is simulated. The characteristics of the heat and mass transfer and fracture propagation mechanism when using SC-CO₂ and H₂O in hot dry rock fracturing are studied, results are shown in Fig. 14.

Then, Zhou and Burbey (2014), and Song W. et al. (2021) studied the influence of fluid properties on fracture propagation behavior by using the cohesive zone model in conjunction with a poro-elasticity model. They found that fluid viscosity is the most significant property, as it greatly affects the hydraulic conductivity and leak-off coefficient. The effect of viscosity can dominate and mask the effect of compressibility in numerical tests.

Yan et al. (2019b) established a fluid-solid coupling model using the extended finite element method (XFEM) to simulate the SC-CO₂ fracturing of coal seam. Through this model, the SC-CO₂ fracturing process is considered as being divided into the SC-CO₂ fracturing stage and the CO₂ phase-transition induced fracturing stage.

Mollaali et al. (2019) adopted the phase field approach to model CO₂ fracturing in porous media. The flow of CO₂, which is considered as a compressible fluid, is modeled by modifying Darcy's law. Several numerical examples are validated and discussed as well. It also indicated that the phase field approach potentially allows complicated modeling of fracture initiation and branching. Another prevalent approach used for CO₂ fracturing is DDM. He et al. (2020) built three-dimensional model of fracture propagation and reservoir rock deformation by combing the DDM and the finite volume method (FVM). On the basis of the model, the influence of geological factors and construction factors on fracture propagation are analyzed during SC-CO₂ fracturing. Afterwards, Zhao et al. (2021) established the CO₂ fracturing model in naturally fractured reservoirs based on the simplified three-dimensional DDM. Through this optimized model, the single fracture characteristics induced by CO₂, slickwater, and gel fracturing in naturally fractured reservoirs and without natural-fracture (NF) reservoirs are analyzed. Then, the effects of NF spacing and length on CO₂ multiple fracturing are studied. Moreover, to investigate CO₂ foam fracturing, a new model based on finite difference and DDM is established by Cong et al. (2022). The model considers not only the effect of temperature-pressure-phase change on CO₂ foam properties, but also the coupling between the influence and fracture propagation. From the calculation model, the effect of CO₂ foam quality, injection temperature and formation parameters on fracture propagation are analyzed. Also, the coupling method can be used for reference in other fields, such as N₂ foam and other water-saving fracturing simulation and wellbore parameters prediction.

In general, numerical research on fracture initiation and propagation with SC-CO₂ fracturing is still in its initial stage. Current numerical methods of SC-CO₂ fracturing are mainly based on two-dimensional models, and only a few models are established in three-dimensional model. Moreover, heat transfer in the CO₂ fracturing process are ignored. Besides, most of the models simulate the propagation characteristic in a relatively simple model (single fracture problem) and fails to represent the field-scale problem with formation anisotropy and existing of natural fractures. Therefore, the numerical research on SC-CO₂ fracturing still has great potential in the future, which needs to be improved and optimized in terms of model accuracy and complexity. Hybrid-based methods will be tendency to simulate CO₂ fracturing, such

as fracturing model based on DDM combined with FVM etc. (He et al., 2020). The main reasons are as follows: (1) the fracturing process involves multiple-field coupling like compressible fluid flow, reservoir damage, and multiphase heat transfer, etc.; (2) the transition from continuum to discontinuum may occur due to progressive insertion of discontinuities such as failure, fracture, fragmentation processes, which motivates the development of combined method.

In addition to the simulation of fracture initiation and propagation, many scholars have studied other processes during CO₂ fracturing through numerical methods, such as the flow and heat transfer mechanism in wellbore and fracture (Yang et al., 2018; Wang et al., 2019; Wang et al., 2019), the interaction mechanism between CO₂ and reservoir rocks and fluids (Jiang et al., 2016; Pan et al., 2018), as well as explored the feasibility of carrying proppant with SC-CO₂ (Hou et al., 2017; Du et al., 2018; Wang et al., 2018a; Zheng et al., 2020) etc. However, these topics are beyond the scope of this review, and we will cover other aspects during SC-CO₂ fracturing in our future work.

3. Principal research results and future challenge on SC-CO₂ fracturing

In this section, the main findings and results obtained through above research with respect to SC-CO₂ fracturing are reviewed, which involving: (1) breakdown pressure when performing SC-CO₂ fracturing; (2) the morphology and related attributes of fracture induced by various fluids; (3) the main mechanism of fracture initiation and propagation during SC-CO₂ fracturing.

3.1. Initiation pressure induced by SC-CO₂ fracturing

3.1.1. Theory description on initiation pressure with SC-CO₂ fracturing

Most traditional criteria about the fracturing initiation pressure are obtained based on the theory of linear elastic fracture mechanics (LEFM). It is expressed that fracture initiation will be happened when the tangential stress reaches the tensile strength of the rock on borehole wall, and the tangential stress σ_θ on borehole wall is expressed in a cylindrical coordinate system as follows (Hubbert and Willis, 1957):

$$\sigma_\theta = \sigma_\theta^{(1)} + \sigma_\theta^{(2)} = \sigma_t \quad (1)$$

where σ_t is the maximum tensile stress; $\sigma_\theta^{(1)}$ is the circumferential stress caused by horizontal principal stresses σ_H and σ_h ; and $\sigma_\theta^{(2)}$ is that caused by wellbore fluid pressure P . The stress of which can be calculated by following formulas:

$$\sigma_\theta^{(1)} = \frac{\sigma_H + \sigma_h}{2} \left(1 + \frac{R^2}{r^2} \right) - \frac{\sigma_H - \sigma_h}{2} \left(1 + 3\frac{R^2}{r^2} \right) \cos(2\theta) \quad (2)$$

$$\sigma_\theta^{(2)} = \frac{R^2}{r^2} P \quad (3)$$

where (r, θ) represents a cylindrical coordinate system; r is the radial distance away from the wall; θ is the tangential angle; R is the wellbore radius. It is notable that $\sigma_\theta^{(1)}$ is dependent of θ , and it reaches the maximum value at the direction of the maximum horizontal stress, where $\theta = 0$ and π . Therefore, formation will initiate at $\theta = 0$ and π when P reaches a critical value, which called at initiation pressure P_f . P_f can be obtained by substituting the expressions of Eqs. (2) and (3) into Eq. (1), which is given by:

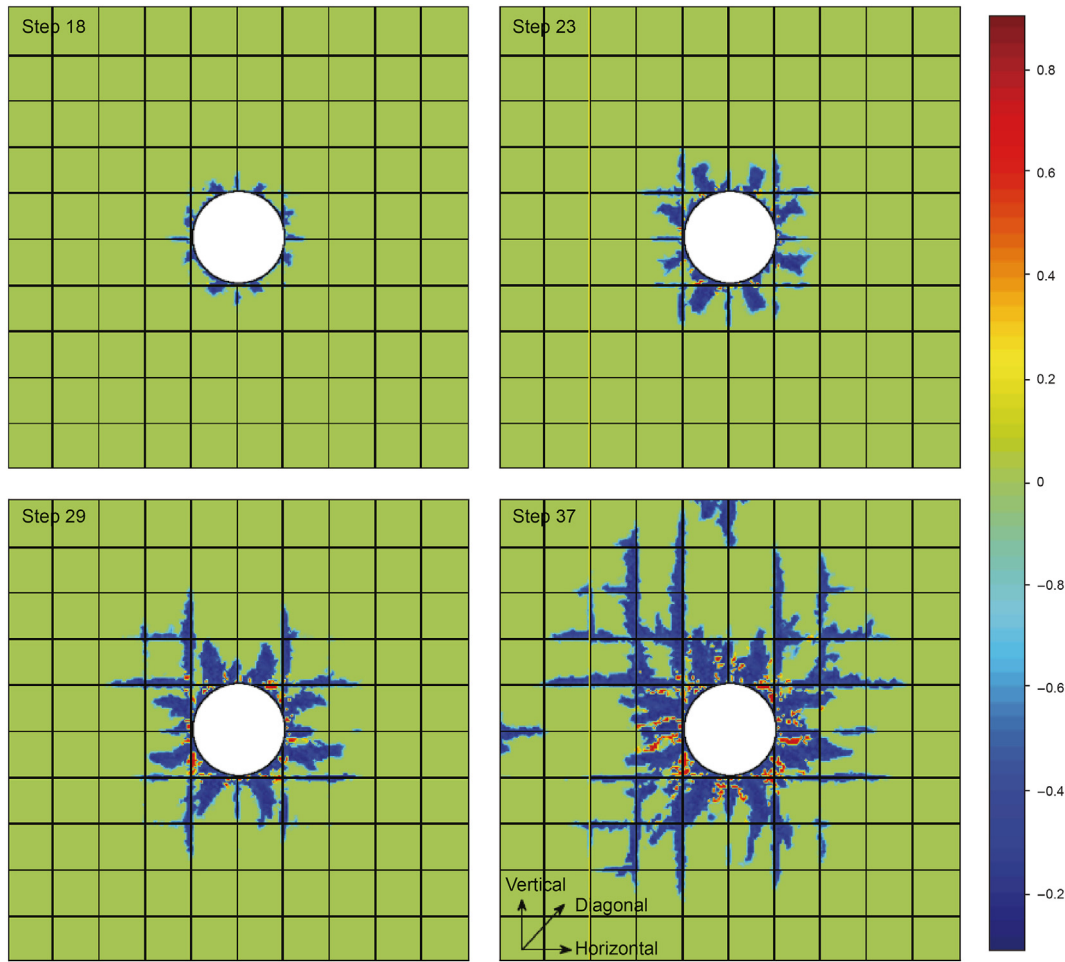


Fig. 13. Distribution and evolution of the fracture in the orthogonal jointed sample (Zhang et al., 2019d).

$$P_f = \sigma_t - (3\sigma_h - \sigma_H) \tag{4}$$

For the case of axisymmetric cylindrical specimen, σ_H and σ_h are two horizontal stresses, equaling confining pressure σ_c . The Hubbert-Willis equation (Hubbert and Willis, 1957) will be derived from Eq. (4), which is:

$$P_f = \sigma_t - 2\sigma_c \tag{5}$$

Above initiation pressure equations represent the extreme case that the rock is completely impermeable, and this criterion ignores the effect of pore pressure. However, SC-CO₂-based fracturing fluid has extremely low viscosity and low surface tension and can penetrate into the rock for a certain depth. The percolation effect cannot be neglected when performing SC-CO₂ fracturing in formations, such as shale and tight reservoir. The SC-CO₂ penetration causes an additional tangential stress $\sigma_\theta^{(3)}$ in compression around the wellbore. The poro-elastic stress $\sigma_\theta^{(3)}$ caused by the radially-varying pore pressure can be calculated by Ito (2008):

$$\sigma_\theta^{(3)} = \frac{\alpha(1-2\nu)}{1-\nu} \left[\frac{1}{r^2} \int_R^r P(r)rdr - P(r) \right] \tag{6}$$

where ν is Poisson's ratio; Biot's coefficient $\alpha = (1 - C_r/C_b)$, C_r and C_b are the rock matrix compressibility and rock bulk compressibility, respectively (Biot and Willis, 1957), and $P(r)$ is the pore pressure at the distance r from the center of wellbore. The

additional pore pressure of fracturing fluid in the infiltration area not only cause an additional circumferential stress $\sigma_\theta^{(3)}$, but also reduce the strength of rocks. Based on the Terzaghi effective stress law (Jaeger, 1963), then Eq. (1) should be changed as follow:

$$\sigma_\theta^{(1)} + \sigma_\theta^{(2)} + \sigma_\theta^{(3)} = \sigma_t - P \quad (\text{at } r=R) \tag{7}$$

Haimson and Fairhurst (1967) pointed out that fracture initiates on the borehole wall (where $r = R$), so $P(r)$ and $\sigma_\theta^{(3)}$ equal P and $\frac{\alpha(1-2\nu)}{1-\nu}P$, respectively. And $\sigma_\theta^{(3)}$ at $r = R$ is determined by just the wellbore pressure P but independent of pore pressure distribution at inside of rock. Then initiation pressure can be derived by substituting those expressions of P and $\sigma_\theta^{(3)}$ into Eq. (7), given by the following expression (Zhang et al., 2017a; Jiang et al., 2018; Ranjith et al., 2019):

$$P_f = \frac{\sigma_t - (3\sigma_h - \sigma_H)}{2 - \frac{\alpha(1-2\nu)}{1-\nu}} \tag{8}$$

Eq. (8) is appropriate for estimating initiation pressure for SC-CO₂ fracturing. Comparing with Eq. (4) without considering poro-elastic effects, the equation of initiation pressure for SC-CO₂ fracturing is different by a factor of $1/(2 - A)$, where $A = \frac{\alpha(1-2\nu)}{1-\nu}$. Generally, $\varphi \leq \alpha \leq 1$ (φ is the porosity of rock) and $0 \leq \nu \leq 0.5$ for rock, so A can be obtained in range of $0 \leq A \leq 1$. Therefore, the factor of $1/(2 - A)$ takes a value between 0.5 and 1. This theory implies that initiation pressure for SC-CO₂ fracturing should be

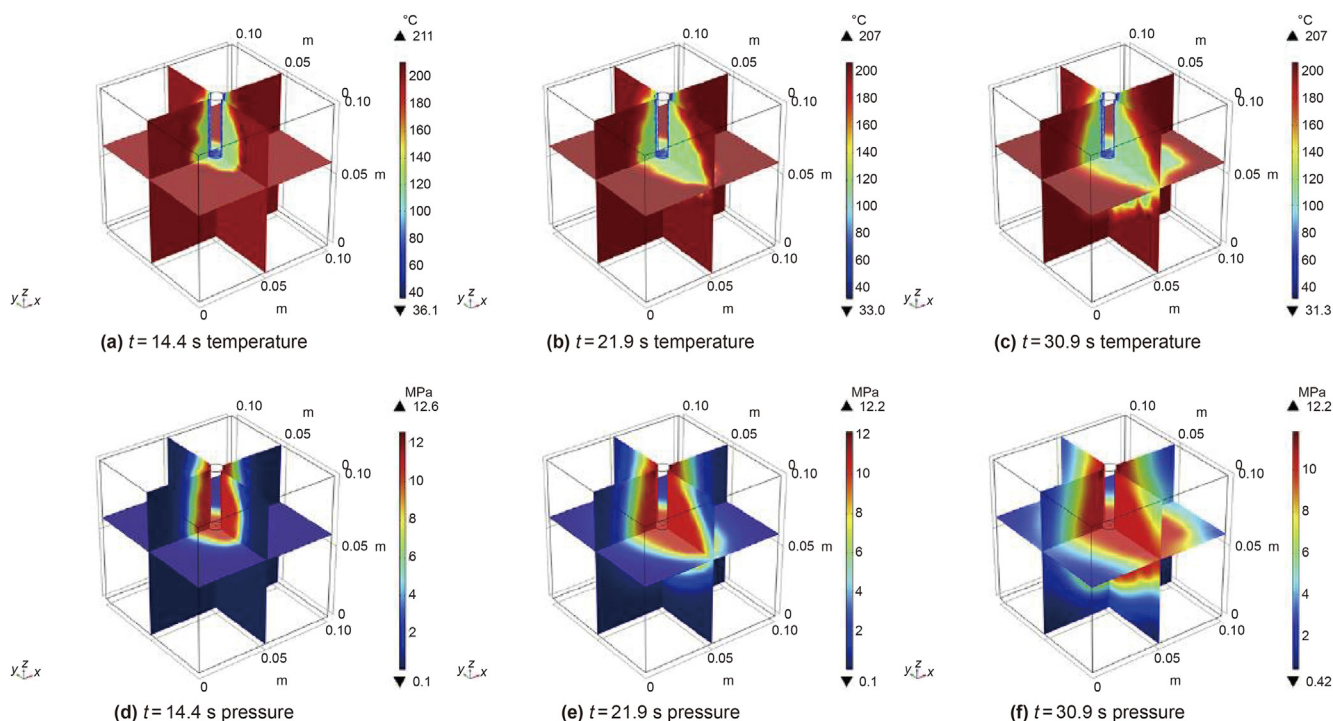


Fig. 14. Evolution of temperature and seepage field when using SC-CO₂ fracturing in HDR (Zhang et al., 2021).

smaller than that for hydraulic fracturing (Deng et al., 2018; Isaka et al., 2019).

3.1.2. Results on initiation pressure during SC-CO₂ fracturing

In this section, the initiation pressure of rock induced by different fluids will be discussed. The formulas of initiation pressure described previously are validated through these fundamental research as well. Then, impacts of main parameters in geology and engineering, such as *in-situ* stress, temperature, anisotropic behavior, natural fracture, pumping rate, perforation angle etc., on initiation pressure during SC-CO₂ fracturing are analyzed.

Initially, Bennour et al. (2015), Ishida et al. (2004, 2012), Inui et al. (2014), and Chen et al. (2015) first investigated the effect of fluid viscosity on fracture initiation with viscous oil, water, L-CO₂ and SC-CO₂ (as listed in Table S1 in Supplementary Material). The results indicated that SC-CO₂ has the lowest initiation pressure among these fluids, followed by L-CO₂, and viscous oil. Viscous oil has the highest fracture initiation pressure. The result is consistent with theoretical prediction by Eqs. (4) and (8), and also validated through a series of experiments and numerical simulation studies (Zhou et al., 2016; Zhang et al., 2017b; Wang et al., 2018b). Alpern et al. (2012) used various gas such as helium (He), nitrogen (N₂), carbon dioxide (CO₂), argon (Ar), sulfur hexafluoride (SF₆) to conduct fracturing experiments on PMMA material, their results suggested that fluids with a higher molecular weight will lead a higher initiation pressure for PMMA sample. Afterwards, Li et al. (2016), Yang et al. (2021a) verified this by conducting fracturing experiments on shale samples using N₂ and CO₂. In recent years, Li et al. (2019), Zou et al. (2018), Zhou et al. (2018a) performed comparison experiments with SC-CO₂ and other common fracturing fluids such as guar gum and gel. They found that SC-CO₂ fracturing had the lowest fracture initiation pressure as well. All the studies indicate that CO₂-based fracturing fluid has a nearly 20%–50% lower initiation pressure than high-viscosity fluids, such as oil-based or water-based fracturing fluids (Ishida et al., 2012; Zhang

et al., 2017a). That is because CO₂-based fluids have low/ultralow viscosity and high diffusivity. It is more capable of increasing pore pressure and reducing effective normal stress than water-based and oil-based fluids, thus causing the rock failure at lower pressures. Besides, it is worth noting that the entire water fracturing process takes much shorter time than that of the SC-CO₂ fracturing process (as shown in Fig. 15) (Ishida et al., 2013; Zhang et al., 2017a; Deng et al., 2018). This could be attributed to lower compressibility of water compared to SC-CO₂ (Motakabbir and Berkowitz, 1990; Yang et al., 2021b).

In addition to the influence of fluid properties on fracture initiation, the geological conditions, such as *in-situ* stress, temperature, anisotropic behavior of formation, etc., also significantly impact on hydraulic fracturing performance. Firstly, to investigate the effect of *in-situ* stress on fracture initiation. Lots of fracturing experiments with SC-CO₂ under various stress conditions have been conducted (Bennour et al., 2015; Zhao et al., 2018). In general, the fracture initiation pressure increases gradually with increasing of applied stress on sample (Zhao et al., 2018; Yang et al., 2021b). And a higher contrast of stress between maximum and minimum horizontal principal stresses can result in a lower breakdown pressure (Jiang et al., 2018; Zhang et al., 2019a; Wang et al., 2017a). Furthermore, Li et al. (2016) and Yang et al. (2021b) studied the effect of stress status of cylinder specimen on breakdown pressure during SC-CO₂ fracturing. It can be seen from Fig. 16 that the initiation pressure is a linear function of the minimum principal stress (confining or axial stress) (Isaka et al., 2019). The linear relationship indicates that the fracture initiation pressure depends both on rock tensile strength and least principal stress.

Moreover, the fracture propagation usually exhibits anisotropic behavior due to complex sedimentary structures of rock sample. To understand the effect of bedding orientation on fracture initiation pressure. Shale, granite and tuff specimens with different bedding plane angles (BPA, which is defined as the angle between the coring direction and the direction perpendicular to bedding plane) were

collected for SC-CO₂ fracturing experiments (Zhang et al., 2019b; Kizaki et al., 2012). Results indicate that the specimen with BPA of 0° shows the highest initiation pressure, while the specimen with BPA of 90° shows the lowest initiation pressure. Initiation pressures of the rest specimens fluctuate in a certain range. In general, it shows a decreasing tendency of the initiation pressure with increasing of the bedding plane angle (He et al., 2019). On the other hand, natural fracture is an important factor that influences fracture initiation pressure. Wang et al. (2017b) and Deng et al. (2018)'s studies implied that SC-CO₂ fracturing on shale samples with natural fractures have much lower initiation pressures than poro-elastic model predictions (Eq. (8)). The reason may be that if pre-existing fractures are accessible to the injecting fluids, the initiation pressure will be reduced as the induced fractures will propagate along the pre-existing fractures.

As mentioned above, fluid viscosity can greatly affect fracturing behavior. Moreover, the viscosity of CO₂ is sensitive to temperature and pressure of subsurface formation (Motakabbir and Berkowitz, 1990). So, the effect of temperature on fracture initiation pressure when conducting SC-CO₂ fracturing should be investigated as well. According to results obtained from Zhou et al. (2019) and Isaka et al. (2019), the initiation pressure is decreasing with an increase in temperature. The observed reduction in initiation pressure is mainly due to the viscosity reduction and thermally induced rock strength deterioration with the increase in temperature (Wang et al., 2017b; Isaka et al., 2019).

The fluid injection rate has influence on fracture initiation as well. Research conducted by Ha et al. (2017, 2018) and Zhang et al. (2019b) showed that initiation pressure decreases with the decreasing of the injection rate of SC-CO₂. In the research on hot dry rock (HDR) fracturing with SC-CO₂, Zhang et al. (2021) concluded that the cryogenic induced thermal stress is essential for the generation of fracture network, which can significantly reduce the fracture initiation pressure. And, with the increase in injection mass flux, the rapid accumulation of fracturing fluid would lead to a sharp increase in pressure, which may result in the temperature increase of fracturing fluid and the reduction of cooling efficiency to rock. So, it also suggested that a lower injection rate is more conducive to cryogenic-induced thermal stress. Furthermore, Chen et al. (2019) explored the effect of perforation angle on fracturing with synthetic cement sample, they found that initiation pressure increases as the perforation angle increases for both hydraulic fracturing and SC-CO₂ fracturing.

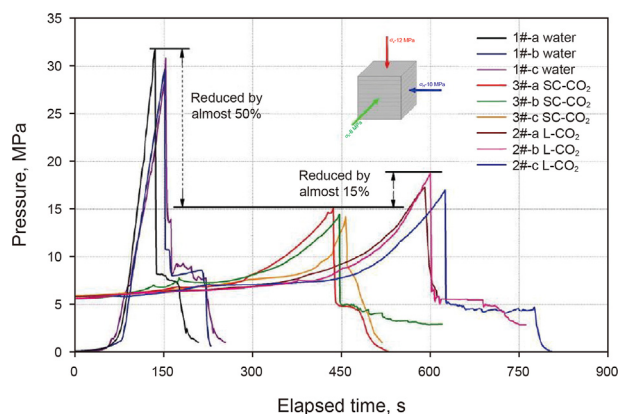


Fig. 15. Pressure curve versus time induced by water and L-/SC-CO₂ (Zhang et al., 2017a).

3.2. Fracture morphology and attributes created by SC-CO₂

To figure out the difference between SC-CO₂ and conventional hydraulic fracturing, fracture morphology and related geometric properties are the most critical characteristics to be analyzed. According to what we reviewed in Section 2 and Table S1 in Supplementary Material, numerous techniques have been used to explore the fracture morphology induced by various fluids. In this section, the fracture distribution, related geometric properties including tortuosity, roughness and complexity are qualitatively and quantitatively analyzed. Then, the effect of geological factors such as *in-situ* stress, natural fractures, bedding planes and temperature etc., on fracture morphology are also discussed.

Initially, Ishida et al. concluded that the distribution of AE sources is affected by the viscosity of fracturing fluid (Ishida et al., 2004, 2012, 2013; Warpinski et al., 2005). The AE sources measured from the SC- and L-CO₂ fracturing experiments distributed in larger areas with three-dimensional pattern than the AE sources from water fracturing. It indicates that the injection of low viscosity fluid such as SC-CO₂ can generate complex fractures with multiple branches, while approximately single fracture was created by injecting the water (Kizaki et al., 2012). Zhou et al. (2016), Li et al. (2016), Zou et al. (2018), and Yang et al. (2021a) conducted hydraulic experiments to validate this result that the lower-viscosity fluid would create more complex fracture network with multiple branches, which can be observed from fracture reconstruction model on the base of CT images in Fig. 12. Also, quantitative results of fracture aperture distribution (Fig. 17 obtained from CT scanning image) suggest that the fracture induced by SC-CO₂ is narrower than that induced by the oil- and water-based fracturing fluids of high viscosity (Ha et al., 2018; Li et al., 2019; Yang et al., 2021a). By analyzing the polarities of P-wave initial motion, it is found that the low-viscosity fluid such as SC-CO₂ induces shear dominant fractures, while the high-viscosity fluid induces tensile dominant fractures (Inui et al., 2014; Chen et al., 2015; Bennour et al., 2015; Zhou et al., 2016, 2019).

As shown in Fig. 7, the images taken from a petrographic microscope show that the fractures induced by SC-CO₂ propagated mainly along the grain boundaries of the constituent minerals, and consequently, resulted in the formation of inter-granular fractures. Many small fractures were also observed in the direction of the maximum principal stress. In contrast, the fractures induced by oil and water injection cut through the many mineral grains and then intra-granular fractures were formed. And they propagated almost along the direction of the maximum principal stress without bending. It implies that low viscosity fluid tends to propagate along rock defects, such as the boundary of grains, weak planes or natural fractures, thereby inducing more complex fracture network (Bennour et al., 2015; Chen et al., 2015; Ishida et al., 2016; Zhou et al., 2018a; Jia et al., 2018).

Moreover, many advanced approaches to analyze fractures listed in Table 1 are adopted to quantitatively characterize fracture attributes. Tortuosity, roughness and complexity are three crucial properties to describe fracture surface topography. Fracture tortuosity τ is widely used to quantify the curvature degree of fractures, and it is defined as the ratio between the total fracture length L_f and the shortest length of the two ends of a fracture L (Zhao et al., 2018; Zhou et al., 2018b; Chen et al., 2015). Under the same experimental condition, the tortuosity of the main fracture induced by SC-CO₂ fracturing is higher than that induced by water fracturing (Jia et al., 2018; He et al., 2019; Ranjith et al., 2019), suggesting that SC-CO₂ is more effective in developing tortuous fractures. Secondly, the area ratio (AR), standard deviation and a series of profile height parameters (S_a , S_q , S_z , etc.), are introduced to evaluate roughness of the main fracture surfaces. Quantitative results obtained from

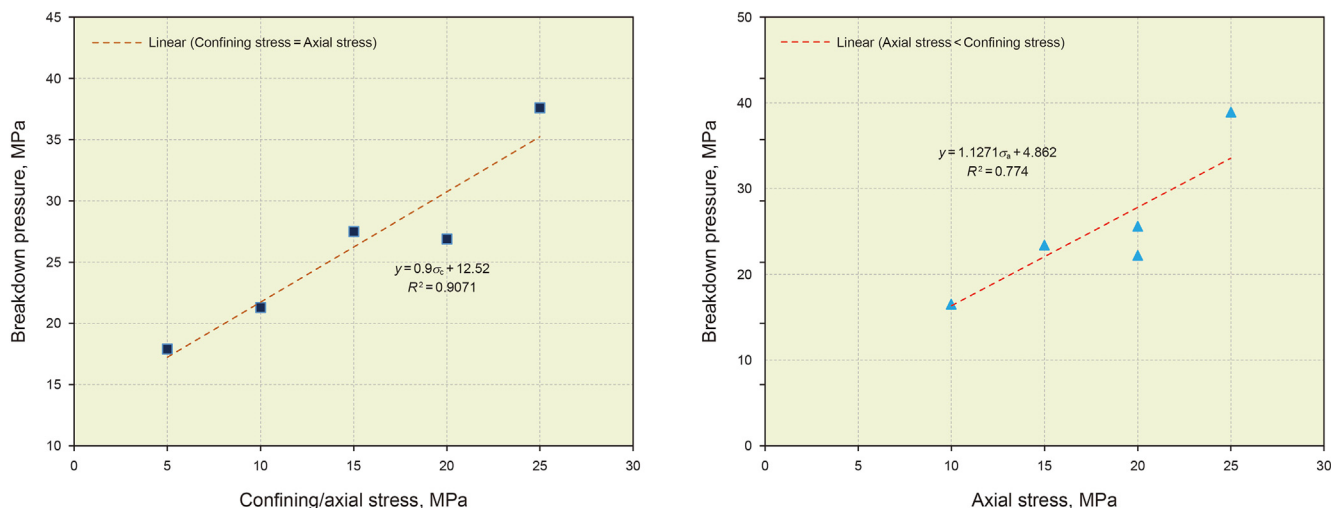


Fig. 16. Breakdown pressure varied with minimum principal stress: (a) effect of confining stress, (b) effect of axial stress (Yang et al., 2021b).

scanning profilometry and CT images etc. (partially depicted from Fig. 9) imply that the main fracture surface created by SC-CO₂ is much rougher than that created by water (Li et al., 2016; Zhao et al., 2018; Zhang et al., 2020; Yang et al., 2021a; Jia et al., 2018; Zhang et al., 2019a). Eventually, the complexity of fracture is quantitatively characterized by parameters such as fractal dimension (FD), the number of fractures, stimulated fracture area, etc. The results are consistent with the qualitative results obtained above. Fractures induced by SC-CO₂ exhibit more complex geometric characteristics through more fracture branches and higher FD etc. (Zhang et al., 2017a; Zou et al., 2018; Jia et al., 2018; Yang et al., 2021a), the similar fracture morphology characteristics is also obtained from THMD coupling model by Zhang et al. (2021).

Besides, geological factors of subsurface formation such as *in-situ* stress, natural fractures, bedding planes and temperature etc., also have great influences on fracture morphology during SC-CO₂. The *in-situ* stress is the principal factor to control fracture propagation. It mainly depends on which factor has a greater influence on the fracture propagation. Classical fracture mechanics theories indicate that fracture is prone to propagate along the direction that is perpendicular to the direction of the minimum principal stress. When higher confining stress value and stress differences are exerted on rock, the major induced fracture planes become much smoother and are perpendicular to the minimum horizontal stress direction (Wang et al., 2017a), the number of macro-fractures reduces and fracture paths deflect (Zhang et al., 2017a). When experimental samples are with well-developed natural bedding structure, the SC-CO₂-induced fractures mainly propagate along natural fractures, weakly bonded bedding planes and interbeds with crossing beddings (Zhao et al., 2018; Zhang et al., 2017a; Wang et al., 2017b; Jiang et al., 2018). And, due to the existence of natural bedding planes, different patterns of fracture propagation may occur in shale fracturing, including deflection, branching, and approaching (Zhang et al., 2019a). So, under complicated formation environment, SC-CO₂ fracturing tends to create fractures in multiple patterns.

To explore the influence of temperature on SC-CO₂ fracturing, hot dry rock and synthetic concrete were prepared to perform experiments in different temperatures (Isaka et al., 2019; Zhou et al., 2019). Their conclusions suggest that the temperature difference between cool fracturing fluid and hot rock results in the cryogenic induced thermal stress, which can reduce the fracture initiation pressure. Moreover, the temperature influences the

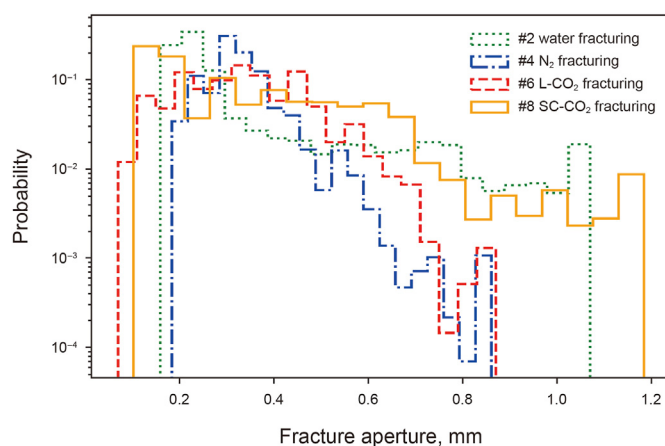


Fig. 17. The distribution of fracture aperture induced by different fluids (Yang et al., 2021a).

morphology of induced fractures significantly (Zhang et al., 2021). The fracture morphology can be classified into the single fracture which propagates obliquely or along the principal stress direction, and the fracture network with the increasing of temperature. And the density of induced fractures decreases, but the tortuosity of fractures increases with an increase in temperature, it suggests the massive development of thin narrow fractures under high-temperature conditions (as shown in Fig. 18) (Isaka et al., 2019).

3.3. Fracturing mechanism of SC-CO₂

Through a series of experimental and numerical studies of SC-CO₂ fracturing, results indicate that the underlying fracturing mechanism of SC-CO₂ is different from the conventional fracturing. The main mechanisms of SC-CO₂ fracturing will be summarized in this section. Firstly, the difference in fracturing results of SC-CO₂ and water-based or oil-based fracturing fluid seems to be significantly affected by the viscosity. According to the theory of Espinoza and Santamarina (2010), capillary effects dominate the process that how fluid (SC-CO₂ and H₂O) invades into the rock matrix. In such a case, the pore structure serves as a significant influencing factor for the process. For a particular pore structure, the critical breakthrough/entry pressure (P_c) is determined by the pressure-

independent interfacial tension (δ) and contact angle (θ). Thus, the pressure required for fluid to enter a pore throat can be calculated as:

$$P_c = \frac{4\delta\cos\theta}{d} \quad (9)$$

where d is the critical pore throat size that fluid may enter.

Eq. (9) suggests that the critical pore throat size is positively correlated with interfacial tension and the cosine of the contact angle. Whereas, the interfacial tension and contact angle of SC-CO₂ are much lower than that of water under the same condition. Meanwhile, a low-viscosity fluid of SC-CO₂ leads to a low flow resistance within a hydraulic fracture (Zou et al., 2018). Thus, under the same injection pressure, SC-CO₂ could enter the pore throats with a smaller pore throat size while H₂O will be excluded (Fig. 19). As a result, mineral grains between two secondary or minor fractures are possibly peeled off from the fracture surface. It is able to make shear sliding in shale to form micro-fractures and secondary fractures. And, the SC-CO₂ may expand the pores and eventually lead to the opening of a fracture (He et al., 2019; Chen et al., 2015). These induced micro-fractures enhanced the complexity of the hydraulic fractures and the porosity of formation, providing additional micro-flow channels for oil and gas (Zhang et al., 2017a; Li et al., 2019). While for the water-based fracturing fluid, the fluid cannot enter those small pore throats and will cut through mineral grains in the process of fracture propagation. It is dominated by tensile failure and limits the creation of micro-fractures and crush of mineral grains (Chen et al., 2015).

Secondly, since the temperature of fracturing fluid is lower than that of formation in the beginning of fracturing. The thermal stress will be introduced when the hot mineral particles contact with cold fluid (Taron and Elsworth, 2009), which will act on the rock in the form of tensile stress (Enayatpour et al., 2019). In reservoir fracturing, the injection pressure generated by fracturing fluid also tends to induce tensile failure, so the thermal stress induced by temperature difference can effectively reduce the fracture initiation pressure. Moreover, because of the low viscosity, SC-CO₂ can easily enter the narrow pore space of rock, increase pore pressure and enhance heat convection. So it will tend to form a fracture network with branches under the comprehensive effects of fluid injection and thermal stress. However, the heat transfer rate of SC-CO₂ is higher than water because its greater specific heat capacity. Thus, the active region of cryogenic induced thermal stress is limited in the vicinity of wellbore when SC-CO₂ injected (Isaka et al., 2019; Zhang et al., 2021).

Furthermore, CO₂ phase transition-induced fracture is a significant mechanism for SC-CO₂ fracturing (Yan et al., 2019a). Compared with conventional hydraulic fracturing, the existence of CO₂ phase transition makes the fracturing mechanism of SC-CO₂ is more complicated and results in a better fracturing performance. To clearly observe fracturing process, Zhou et al. (2018b) conducted fracturing experiments with PMMA material instead of non-transparent rock sample. They also concluded that when fractures start to propagate, SC-CO₂ converts to gas state instantly. The massive energy stored in SC-CO₂ are released to extend initial fractures further during phase change, resulting in a higher fracture propagating speed. The high-speed propagation of fractures would suddenly alter orientation of the stress field. In conclusion, the more external energy is supplied during SC-CO₂ phase change, which is more beneficial to accelerating fracture propagation and generating multi-fractures (Zhou et al., 2016, 2019).

4. Development history of field utilization on SC-CO₂ fracturing

In the 1980s, CO₂ as a fracturing fluid was first applied to oil field, this technology mainly includes CO₂ dry fracturing, CO₂-foam fracturing, etc. (Wamock et al., 1985; Sinal and Lancaster, 1987). In the initial stage, CO₂ dry fracturing was proposed and used in field where CO₂ was injected into the reservoir with sand. The commercial success of this method was first achieved in Canada. Subsequently, this stimulation approach was utilized in oilfield more than 350 wells before 2003 (Gupta, 2003). Fracmaster introduced the technology to the US market after the 1980s and subsequently applied it in the Devonian shale reservoirs in Western Pennsylvania, Texas, and Colorado (Harris et al., 1998). In 1999, 16 wells were selected by the Burlington Company in Mexico to test the feasibility of the liquid CO₂ sand fracturing technology in the entire San Juan Basin (Campbell et al., 2000). The dry CO₂ fracturing technology was also implemented in China. About 50 wells have been operated with liquid CO₂ fracturing in Changqing, Jilin and Yanchang oilfields of China (Wang X. et al., 2014; Meng et al., 2018). Although dry CO₂ fracturing can effectively stimulate unconventional reservoirs, the drawbacks, such as low proppant-carrying capacity and high leak-off volume, also significantly limit its field application (Nianyin et al., 2021). Meanwhile, to improve fracturing performance, the CO₂ foam fracturing was also developed in Canada and US (Craft et al., 1992). In 2000, the field trial was carried out in US for the development of Ohio shale gas. Moreover, in 2002, CO₂ foam fracturing was also applied in the Lewis shale reservoir by the Burlington Company and shows promising results. Currently, the CO₂ foam fracturing technology is relatively mature in the US, Canada, Saudi Arabia, and China (Johnson and Johnson, 2012; Malik et al., 2014; Mahmud et al., 2020; Mojid et al., 2021). However, there are still some limitations to restrict this technology, such as how to ensure the foam stability of fracturing fluid and minimize the formation damage.

With the development and application of SC-CO₂ fracturing technology, people begin to explore the feasibility of this technology in field application. SC-CO₂ fracturing is a special form of dry CO₂ fracturing. The principal difference between the two processes is that CO₂ has reached the supercritical state before reaching the fracture zone (Liu et al., 2014; Nianyin et al., 2021). In 2017, the joint team of China University of Petroleum (Beijing), Wuhan University and Shaanxi Yanchang Petroleum Group, conducted the first field test of SC-CO₂ fracturing for development of shale gas in Shaanxi province, China (Wang He et al., 2020). In the field trial, the depth of the well is 2940 m, and 386 m³ liquid CO₂ were injected both through the tubing and casing. Also, the flow friction, wellbore temperature profile and proppant carrying performance of SC-CO₂ were tested in the field. Results indicated that the CO₂ temperature at the bottom of the wellbore reached the critical temperature at the field conditions. The frictional resistance was higher than traditional hydraulic fracturing, and pressure drop in the nozzle counts a large proportion of the system pressure loss. Moreover, due to the low density and viscosity of SC-CO₂, severe proppant plugging is observed due to low proppant carrying capacity. Thus, the conventional fracturing fluids were utilized to carry proppant eventually. In addition, micro-seismic monitoring results show that the fracture initiation signals induced by SC-CO₂ are complicated and uniformly distributed in all directions in the vicinity of the wellbore. While after switching to hydraulic fracturing, results show that the fracture distributed along the direction of the maximum horizontal principal stress (Fig. 20). It is further proved

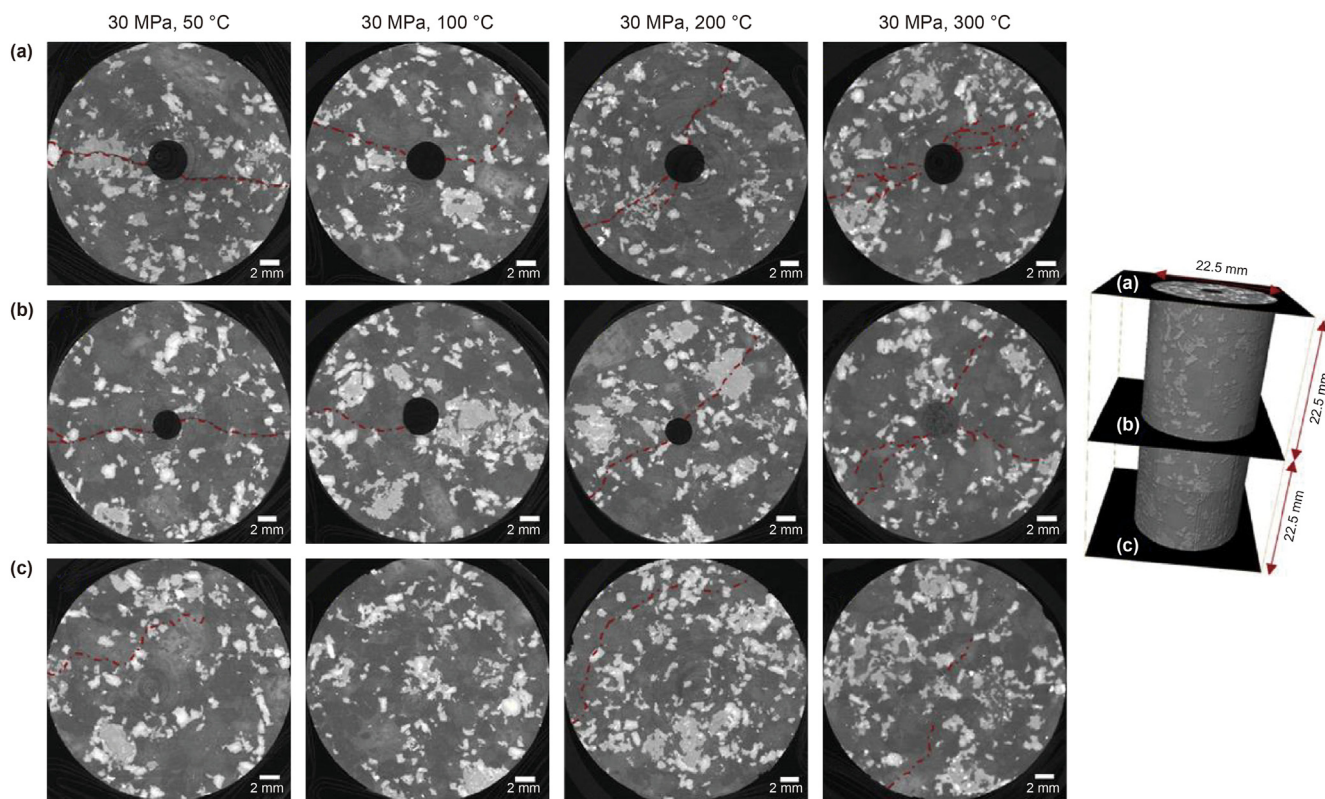


Fig. 18. CT images at different locations of rock specimens fractured by SC-CO₂ at varying temperatures under 30 MPa confining pressure (Isaka et al., 2019).

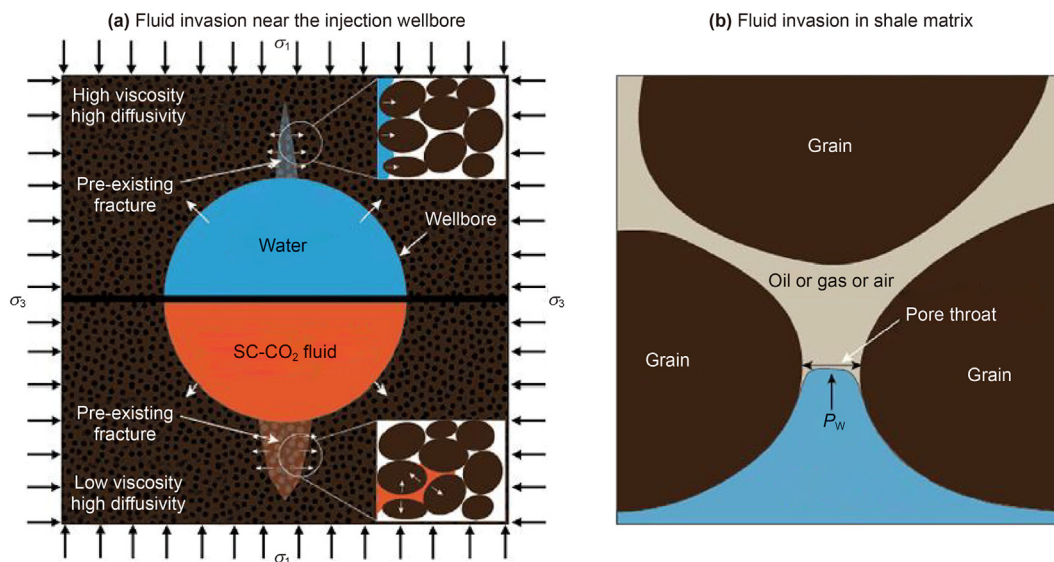


Fig. 19. (a) Fluid invasion near the injection wellbore. Due to the low viscosity and high diffusivity of SC-CO₂, a large affected area is created near pre-existing natural fractures or flow channels. (b) In the area distant from the injection wellbore, capillary effects determine that SC-CO₂ enters pore throats as small as 5.7 nm, while H₂O may only penetrate pore throats larger than 12.9 nm (Jia et al., 2018).

that SC-CO₂ can create a complex fracture network with multiple branches and weakens the dominant role of *in-situ* stress in field scale experiments. In addition, a hybrid fracturing method using both SC-CO₂ and conventional fracturing fluid has been considered as a new fracturing technique due to the limitation of sand-carrying capacity of SC-CO₂. This method is not only able to induce complex fractures using SC-CO₂, but also can pump more proppant into the

fracture network using conventional fracturing fluids (Liu et al., 2014; Zhou et al., 2019; Nianyin et al., 2021). At the same time, some researchers are attempting to enhance the proppant carrying capacity of SC-CO₂ by increasing fluid viscosity based on mechanical or chemical methods (Li et al., 2019).

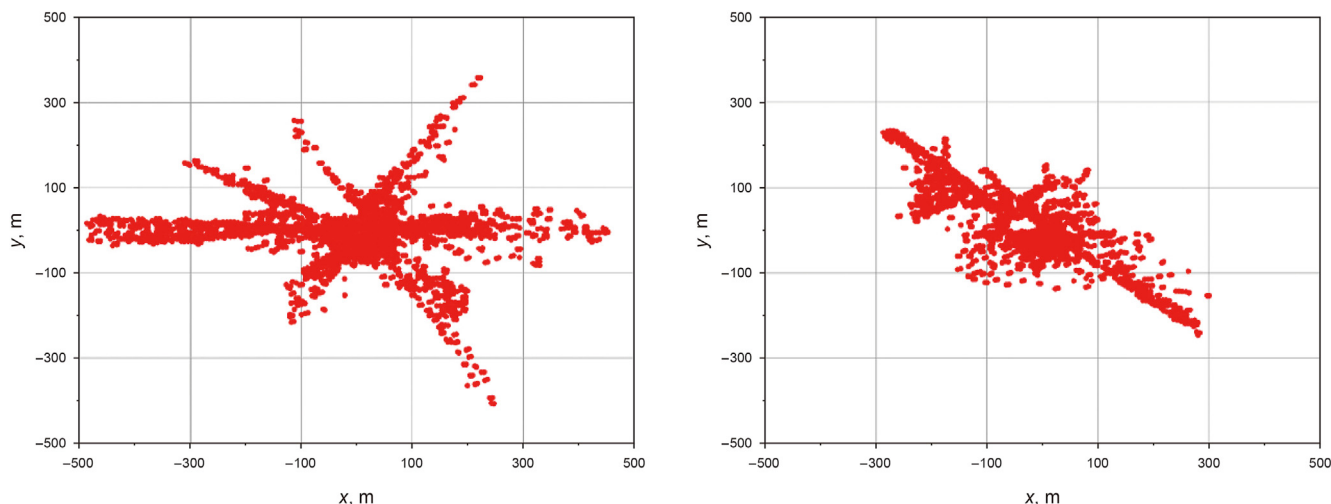


Fig. 20. Comparison of microseismic crack detection (left for SC-CO₂ fracturing; right for hydraulic fracturing) (Wang et al., 2020).

5. Discussion and recommendation on SC-CO₂ fracturing

It is undoubted that hydraulic fracturing with water-based fluid is the most common and effective method in unconventional oil and gas development. However, large-scale utilization of water-based fluids will bring a series of problems to the formation and surface environment, such as reservoir and surface environmental contamination, large consumption of water resources, high cost on treatment of flowback fluid, etc. SC-CO₂, as a particular anhydrous fluid, can effectively solve the above problems, and is considered as a promising alternative fracturing fluid for developing unconventional resource. In recent years, a great number of fundamental studies and field testing on SC-CO₂ fracturing in unconventional reservoirs have been performed. A series of laboratory experiments and numerical simulations were conducted to reveal the mechanisms of fracture initiation and propagation. In this paper, the research status on SC-CO₂ fracturing is reviewed, and the development prospects with respect to laboratory experiment, numerical simulation, field test, etc., are analyzed as well.

At present, the laboratory experiments of SC-CO₂ fracturing are mainly based on pseudo-triaxial and true triaxial experimental systems. SC-CO₂ fracturing experiments on various formations, such as shale, tight sandstone, coal seam, granite and other rock types, are conducted. A series of advanced fracture monitoring and analysis methods are used to analyze fracture characteristics induced by SC-CO₂. In terms of numerical simulation, the common numerical methods for CO₂ fracturing mainly include FEM combined with some secondary development, XFEM, PFM and DDM. However, most of the reported numerical models are based on two dimensions, and three dimensions are rarely considered. Moreover, to save the cost of calculation, many factors, including multi-phase heat transfer, reservoir heterogeneity, etc., are ignored in these fracturing models. Experimental and simulation results show that SC-CO₂ fracturing is less affected by principal stress, and can induce complex fracture networks with multiple fracture branches compared with conventional hydraulic fracturing. It is more likely to produce shear fractures, which is conducive to the formation of fractures with high conductivity. However, under the influence of its own special properties, SC-CO₂ fracturing induced fractures are mostly distributed near the wellbore, with shorter extension distance than hydraulic fracturing. Since its low viscosity of SC-CO₂, conventional fracturing fluids are usually used to carry proppant in field trials. In general, under the background of massive greenhouse gas emissions and worsening global climate, CO₂ as a type of

resource has promising prospects for energy development. Not only does this reduce carbon emissions, but field tests have shown that CO₂ can be retained by more than 30% after injected into the reservoir, achieving partial carbon sequestration as well.

However, in view of current basic research and field test of SC-CO₂ fracturing, there are still some limitations that need to be improved and addressed. Some of the demanding directions for further research and field application are summarized below:

- (1) SC-CO₂ fracturing experimental system: The current fracturing experimental system is mostly designed in the closed environment, so it is difficult to directly observe the propagation of fractures in real time. In the future, a visual/imaging experimental system need to be developed to capture the initiation and propagation of fractures in real time based on high-speed camera and DIC technology.
- (2) Fracture identification and monitoring methods: Fracture analysis methods need to evolve towards real-time monitoring and non-destructive methods. In addition to high-speed imaging system for fracture observations, a triaxial fracturing system can be improved for real-time high-precision CT scanning. The system enables the X-ray penetration test system to capture fracture in real time during fracturing.
- (3) Numerical simulation method of SC-CO₂ fracturing: The hybrid methods based on PFM, DDM, DEM, etc., for multi-physics coupling simulation may be the direction of future development. In addition, heat transfer, local pressure drop and reservoir heterogeneity need to be further considered in the optimized model to improve the fidelity and accuracy, and make it more consistent with original reservoir conditions.
- (4) Field application of SC-CO₂ fracturing: Due to the poor proppant-carrying capacity of pure SC-CO₂, hybrid fracturing with CO₂ and conventional fracturing fluid is commonly used in the field test. This method not only induces complex fractures but also improves proppant-carrying capacity. However, it will increase difficulty and cost as two types of operation equipment and fluids will be deployed. Moreover, some scholars try to increase CO₂ viscosity by physical and chemical methods to improve proppant-carrying performance, but this method also has limitations such as cost increase, reservoir pollution, and impact on fracture networks construction in the first stage (Heller et al., 1985; Trickett et al., 2009; Luo et al., 2015). Thus, a new technology

of enhancing SC-CO₂ proppant-carrying capacity should be developed.

6. Conclusion

Due to its special physical and chemical properties, SC-CO₂ has been considered as anhydrous fracturing fluid to develop unconventional oil and gas resources. In this paper, the state-of-art SC-CO₂ fracturing experimental systems, fracture monitoring methods, numerical simulation methods and field applications are reviewed and discussed. The main mechanisms of fracture initiation and propagation induced by SC-CO₂ are also summarized. Through a series of basic studies and field tests, the feasibility of using SC-CO₂ as fracturing fluid to develop unconventional reservoirs, including shale oil and gas, tight gas, coalbed methane, geothermal resources, etc., has been verified. Results show that hydraulic fracturing with SC-CO₂ has obvious advantages and application prospect compared with conventional hydraulic fracturing. However, due to the differences and complexity of reservoirs and the special properties of SC-CO₂, various issues and challenges will be encountered in SC-CO₂ fracturing process. Based on the current research status, the limitations of basic research and field application are listed, and some suggestions are given as well. It is anticipated that the related research methods will be continuously improved to solve these problems, and the technology of SC-CO₂ fracturing will be widely applied to the field in the future. So as to provide technical support for unconventional resources development and carbon emission reduction projects.

Acknowledgements

This work was supported by the Natural Science Foundation of China (Grant Nos.51922107, 51874318, 51827804 and 41961144026).

Appendix A. Supplementary data

Supplementary data to this article can be found online at <https://doi.org/10.1016/j.petsci.2022.08.029>.

References

Abedini, A., Torabi, F., 2014. On the CO₂ storage potential of cyclic CO₂ injection process for enhanced oil recovery. *Fuel* 124, 14–27. <https://doi.org/10.1016/j.fuel.2014.01.084>.

Advani, S.H., Lee, J., 1982. Finite element model simulations associated with hydraulic fracturing. *SPE J.* 22, 209–218. <https://doi.org/10.2118/8941-PA>.

Alpern, J., Marone, C.J., Elsworth, D., Belmonte, A., Connelly, P., 2012. Exploring the physicochemical processes that govern hydraulic fracture through laboratory experiments. 46th US Rock Mechanics/Geomechanics Symposium. Paper Number: ARMA-2012-678.

Amarasinghe, W., Fjelde, I., Age Rydland, J., Guo, Y., 2020. Effects of permeability on CO₂ dissolution and convection at reservoir temperature and pressure conditions: a visualization study. *Int. J. Greenh. Gas Control* 99, 103082. <https://doi.org/10.1016/j.ijggc.2020.103082>.

Bahrami, H., Rezaee, R., Clennell, B., 2012. Water blocking damage in hydraulically fractured tight sand gas reservoirs: an example from Perth Basin, western Australia. *J. Petrol. Sci. Eng.* 88–89, 100–106. <https://doi.org/10.1016/j.petrol.2012.04.002>.

Bazin, B., Bekri, S., Vizika, O., Herzhaft, B., Aubry, E., 2010. Fracturing in tight gas reservoirs: application of special-core-analysis methods to investigate formation-damage mechanisms. *SPE J.* 15, 969–976. <https://doi.org/10.2118/112460-PA>.

Bennour, Z., Ishida, T., Nagaya, Y., Chen, Y., Nara, Y., Chen, Q., Sekine, K., Nagano, Y., 2015. Crack extension in hydraulic fracturing of shale cores using viscous oil, water, and liquid carbon dioxide. *Rock Mech. Rock Eng.* 48, 1463–1473. <https://doi.org/10.1007/s00603-015-0774-2>.

Bhargava, J., Rehmsström, Å., 1975. High-speed photography for fracture studies of concrete. *Cement Concr. Res.* 5, 239–247. [https://doi.org/10.1016/0008-8846\(75\)90006-X](https://doi.org/10.1016/0008-8846(75)90006-X).

Biot, M.A., Willis, D.G., 1957. The elastic coefficients of the theory of consolidation. *J. Appl. Mech.* 24, 594–601. <https://doi.org/10.1007/s00603-021-02580-2>.

Boone, T.J., Ingraffea, A.R., 1990. A numerical procedure for simulation of hydraulically-driven fracture propagation in poroelastic media. *Int. J. Numer. Anal. Methods GeoMech.* 14, 27–47. <https://doi.org/10.1002/nag.1610140103>.

Brebbia, C., Dominguez, J., 1977. Boundary element methods for potential problems. *Appl. Math. Model.* 1, 372–378. [https://doi.org/10.1016/0307-904X\(77\)90046-4](https://doi.org/10.1016/0307-904X(77)90046-4).

Breede, K., Dzebisashvili, K., Liu, X., Falcone, G., 2013. A systematic review of enhanced (or engineered) geothermal systems: past, present and future. *Geoth. Energy* 1, 4. <https://doi.org/10.1186/2195-9706-1-4>.

Brown, D., 2000. A hot dry rock geothermal energy concept utilizing supercritical CO₂ instead of water. In: *Proceedings of the Twenty-Fifth Workshop on Geothermal Reservoir Engineering*.

Campbell, S., Fairchild, N., Arnold, D., 2000. Liquid CO₂ and sand stimulations in the Lewis shale, San Juan basin, New Mexico: a case study. In: *SPE Rocky Mountain Regional/Low-Permeability Reservoirs Symposium and Exhibition*. <https://doi.org/10.2118/60317-MS>.

Carrier, B., Granet, S., 2012. Numerical modeling of hydraulic fracture problem in permeable medium using cohesive zone model. *Eng. Fract. Mech.* 79, 312–328. <https://doi.org/10.1016/j.engfracmech.2011.11.012>.

Chen, B., Barboza, B., Sun, Y., 2022. A review of hydraulic fracturing simulation. *Arch. Comput. Methods Eng.* 29, 1–58. <https://doi.org/10.1007/s11831-021-09653-z>.

Chen, H., Hu, Y., Kang, Y., Cai, C., Liu, J., Liu, Y., 2019. Fracture initiation and propagation under different perforation orientation angles in supercritical CO₂ fracturing. *J. Petrol. Sci. Eng.* 183, 106403. <https://doi.org/10.1016/j.petrol.2019.106403>.

Chen, Y., Nagaya, Y., Ishida, T., 2015. Observations of fractures induced by hydraulic fracturing in anisotropic granite. *Rock Mech. Rock Eng.* 48, 1455–1461. <https://doi.org/10.1007/s00603-015-0727-9>.

Cong, Z., Li, Y., Pan, Y., Liu, B., Shi, Y., Wei, J., Li, W., 2022. Study on CO₂ foam fracturing model and fracture propagation simulation. *Energy* 238, 121778. <https://doi.org/10.1016/j.energy.2021.121778>.

Craft, J., Waddell, S., McFatrige, D., 1992. CO₂-foam fracturing with methanol successfully stimulates canyon gas sand. *SPE Prod. Eng.* 7, 219–225. <https://doi.org/10.2118/20119-PA>.

Cruse, T., 1968. A direct formulation and numerical solution of the general transient elastodynamic problem. II. *J. Math. Anal. Appl.* 22, 341–355. [https://doi.org/10.1016/0022-247X\(68\)90171-6](https://doi.org/10.1016/0022-247X(68)90171-6).

Cundall, P., 1971. A computer model for simulating progressive large scale movements in blocky rock systems. In: *Symposium of the International Society for Rock Mechanics*, II–8.

Deng, B., Yin, G., Li, M., Zhang, D., Lu, J., Liu, Y., Chen, J., 2018. Feature of fractures induced by hydrofracturing treatment using water and L-CO₂ as fracturing fluids in laboratory experiments. *Fuel* 226, 35–46. <https://doi.org/10.1016/j.fuel.2018.03.162>.

Diamond, S., Mindess, S., 1992. Sem investigations of fracture surfaces using stereo pairs: I. Fracture surfaces of rock and of cement paste. *Cement Concr. Res.* 22, 67–78. [https://doi.org/10.1016/0008-8846\(92\)90137-K](https://doi.org/10.1016/0008-8846(92)90137-K).

Dong, C., de Pater, C., 2001. Numerical implementation of displacement discontinuity method and its application in hydraulic fracturing. *Comput. Methods Appl. Mech. Eng.* 191, 745–760. [https://doi.org/10.1016/S0045-7825\(01\)00273-0](https://doi.org/10.1016/S0045-7825(01)00273-0).

Du, M., Sun, X., Dai, C., Li, H., Wang, T., Xu, Z., Zhao, M., Guan, B., Liu, P., 2018. Laboratory experiment on a toluene-polydimethyl silicone thickened supercritical carbon dioxide fracturing fluid. *J. Petrol. Sci. Eng.* 166, 369–374. <https://doi.org/10.1016/j.petrol.2018.03.039>.

Edwards, R.W.J., Celia, M.A., 2018. Infrastructure to enable deployment of carbon capture, utilization, and storage in the United States. *Proc. Natl. Acad. Sci. USA* 115, E8815–E8824. <https://doi.org/10.1073/pnas.1806504115>.

EIA, 2017. International Energy Outlook 2017. <http://www.eia.gov/ieo>.

Enayatpour, S., van Oort, E., Patzek, T., 2019. Thermal cooling to improve hydraulic fracturing efficiency and hydrocarbon production in shales. *J. Nat. Gas Sci. Eng.* 62, 184–201. <https://doi.org/10.1016/j.jngse.2018.12.008>.

Espinoza, D.N., Santamarina, J.C., 2010. Water-CO₂-mineral systems: Interfacial tension, contact angle, and diffusion—implications to CO₂ geological storage. *Water Resources Research*, vol. 46. <https://doi.org/10.1029/2009WR008634>.

Faruque Hasan, M., First, E.L., Boukouvala, F., Floudas, C.A., 2014. A novel framework for carbon capture, utilization, and sequestration, CCUS. *Comput. Aided Chem. Eng.* 34, 98–107. <https://doi.org/10.1016/B978-0-444-63433-7.50011-0>.

Gonçalves da Silva, B., Einstein, H., 2018. Physical processes involved in the laboratory hydraulic fracturing of granite: visual observations and interpretation. *Eng. Fract. Mech.* 191, 125–142. <https://doi.org/10.1016/j.engfracmech.2018.01.011>.

Gregory, K.B., Vidic, R.D., Dzombak, D.A., 2011. Water management challenges associated with the production of shale gas by hydraulic fracturing. *Elements* 7, 181–186. <https://doi.org/10.2113/gselements.7.3.181>.

Gupta, D., 2003. Field application of unconventional foam technology: extension of liquid CO₂ technology. In: *SPE Annual Technical Conference and Exhibition*. <https://doi.org/10.2118/84119-MS>.

Gupta, P., Duarte, C.A., 2014. Simulation of non-planar three-dimensional hydraulic fracture propagation. *Int. J. Numer. Anal. Methods GeoMech.* 38, 1397–1430. <https://doi.org/10.1002/nag.2305>.

Guo, R., Dalton, L., Fan, M., McClure, J., Zeng, L., Crandall, D., Chen, C., 2020. The role of the spatial heterogeneity and correlation length of surface wettability on two-phase flow in a CO₂-water-rock system. *Adv. Water Resour.* 146, 103763. <https://doi.org/10.1016/j.advwatres.2020.103763>.

- Guo, R., Dalton, L., Wang, H., McClure, J., Crandall, D., Chen, C., 2022. Role of heterogeneous surface wettability on immiscible displacement, capillary pressure, and relative permeability in a CO₂-brine-rock system. *Adv. Water Resour.* e104226.
- Ha, S.J., Choo, J., Yun, T.S., 2018. Liquid CO₂ fracturing: effect of fluid permeation on the breakdown pressure and cracking behavior. *Rock Mech. Rock Eng.* 51, 3407–3420. <https://doi.org/10.1007/s00603-018-1542-x>.
- Ha, S.J., Yun, T.S., Kim, K.Y., Jung, S.G., 2017. Experimental study of pumping rate effect on hydraulic fracturing of cement paste and mortar. *Rock Mech. Rock Eng.* 50, 3115–3119. <https://doi.org/10.1007/s00603-017-1276-1>.
- Haimson, B., Fairhurst, C., 1967. Initiation and extension of hydraulic fractures in rocks. *SPE J.* 7, 310–318. <https://doi.org/10.2118/1710-PA>.
- Hamstad, M.A., 1986. A review: acoustic emission, a tool for composite-materials studies. *Exp. Mech.* 26, 7–13. <https://doi.org/10.1007/BF02319949>.
- Harris, R.P., Ammer, J., Pekot, L.J., Arnold, D.L., 1998. Liquid carbon dioxide fracturing for increasing gas storage deliverability. In: SPE Eastern Regional Meeting. <https://doi.org/10.2118/51066-MS>.
- Hattori, G., Trevelyan, J., Augarde, C.E., Coombs, W.M., Aplin, A.C., 2017. Numerical simulation of fracturing in shale rocks: current state and future approaches. *Arch. Comput. Methods Eng.* 24, 281–317. <https://doi.org/10.1007/s11831-016-9169-0>.
- He, J., Zhang, Y., Li, X., Wan, X., 2019. Experimental investigation on the fractures induced by hydraulic fracturing using freshwater and supercritical CO₂ in shale under uniaxial stress. *Rock Mech. Rock Eng.* 52, 3585–3596. <https://doi.org/10.1007/s00603-019-01820-w>.
- He, Y., Yang, Z., Jiang, Y., Li, X., Zhang, Y., Song, R., 2020. A full three-dimensional fracture propagation model for supercritical carbon dioxide fracturing. *Energy Sci. Eng.* 8, 2894–2906. <https://doi.org/10.1002/ese3.709>.
- Heller, J.P., Dandge, D.K., Card, R.J., Donaruma, L.G., 1985. Direct thickeners for mobility control of CO₂ floods. *SPE J.* 25, 679–686. <https://doi.org/10.2118/11789-PA>.
- Hirata, T., Satoh, T., Ito, K., 1987. Fractal structure of spatial distribution of microfracturing in rock. *Geophys. J. Int.* 90, 369–374. <https://doi.org/10.1111/j.1365-246X.1987.tb00732.x>.
- Hou, L., Jiang, T., Liu, H., Geng, X., Sun, B., Li, G., Meng, S., 2017. An evaluation method of supercritical CO₂ thickening result for particle transporting. *J. CO₂ Util.* 21, 247–252. <https://doi.org/10.1016/j.jcou.2017.07.023>.
- Hou, P., Gao, F., Ju, Y., Yang, Y., Gao, Y., Liu, J., 2017. Effect of water and nitrogen fracturing fluids on initiation and extension of fracture in hydraulic fracturing of porous rock. *J. Nat. Gas Sci. Eng.* 45, 38–52. <https://doi.org/10.1016/j.jngse.2017.05.012>.
- Hou, Z., Xie, H., Zhou, H., Were, P., Kolditz, O., 2015. Unconventional gas resources in China. *Environ. Earth Sci.* 73, 5785–5789. <https://doi.org/10.1007/s12665-015-4393-8>.
- Hu, Y., Liu, F., Hu, Y., Kang, Y., Chen, H., Liu, J., 2019. Propagation characteristics of supercritical carbon dioxide induced fractures under true tri-axial stresses. *Energies* 12, 4229. <https://doi.org/10.3390/en12224229>.
- Hubbert, M.K., Willis, D.G., 1957. Mechanics of hydraulic fracturing. *Transactions of the AIME* 210, 153–168. <https://doi.org/10.2118/686-G>.
- Inui, S., Ishida, T., Nagaya, Y., Nara, Y., Chen, Y., Chen, Q., 2014. AE monitoring of hydraulic fracturing experiments in granite blocks using supercritical CO₂, water and viscous oil. In: 48th U.S. Rock Mechanics/Geomechanics Symposium, ARMA-2014-7163.
- Isaka, B.A., Ranjith, P., Rathnaweera, T., Wanniarachchi, W., Kumari, W., Haque, A., 2019. Testing the frackability of granite using supercritical carbon dioxide: insights into geothermal energy systems. *J. CO₂ Util.* 34, 180–197. <https://doi.org/10.1016/j.jcou.2019.06.009>.
- Ishida, T., Chen, Q., Mizuta, Y., Roegiers, J.C., 2004. Influence of fluid viscosity on the hydraulic fracturing mechanism. *J. Energy Resour. Technol.* 126, 190–200. <https://doi.org/10.1115/1.1791651>.
- Ishida, T., Aoyagi, K., Niwa, T., Chen, Y., Murata, S., Chen, Q., Nakayama, Y., 2012. Acoustic emission monitoring of hydraulic fracturing laboratory experiment with supercritical and liquid CO₂. *Geophys. Res. Lett.* 39, 16309. <https://doi.org/10.1029/2012GL052788>, 16309.
- Ishida, T., Nagaya, Y., Inui, S., Aoyagi, K., Nara, Y., Chen, Y., Chen, Q., Nakayama, Y., 2013. AE monitoring of hydraulic fracturing experiments conducted using CO₂ and water. In: ISRM International Symposium - EUROCK 2013. Paper Number: ISRM-EUROCK-2013-149.
- Ishida, T., Chen, Y., Bennour, Z., Yamashita, H., Inui, S., Nagaya, Y., Naoi, M., Chen, Q., Nakayama, Y., Nagano, Y., 2016. Features of CO₂ fracturing deduced from acoustic emission and microscopy in laboratory experiments. *J. Geophys. Res.* 121, 8080–8098. <https://doi.org/10.1002/2016JB013365>.
- Ishida, T., Desaki, S., Yamashita, H., Inui, S., Naoi, M., Fujii, H., Katayama, T., 2017. Injection of supercritical carbon dioxide into granitic rock and its acoustic emission monitoring. *Procedia Eng.* 191, 476–482. <https://doi.org/10.1016/j.proeng.2017.05.206>.
- Ishida, T., Desaki, S., Kishimoto, Y., Naoi, M., Fujii, H., 2021. Acoustic emission monitoring of hydraulic fracturing using carbon dioxide in a small-scale field experiment. *Int. J. Rock Mech. Min. Sci.* 141, 104712. <https://doi.org/10.1016/j.ijrmm.2021.104712>.
- Ito, T., 2008. Effect of pore pressure gradient on fracture initiation in fluid saturated porous media: *Rock. Eng. Fract. Mech.* 75, 1753–1762. <https://doi.org/10.1016/j.engfracmech.2007.03.028>.
- Jackson, R., 2013. Environmental dimensions of shale gas extraction and stray gas migration. *Bull. Am. Phys. Soc.* 2013.
- Jaeger, J.C., 1963. Extension failures in rocks subject to fluid pressure. *J. Geophys. Res.* 68, 6066–6067. <https://doi.org/10.1029/JZ068i021p06066>.
- Jia, B., Tsau, J.S., Barati, R., 2019. A review of the current progress of CO₂ injection EOR and carbon storage in shale oil reservoirs. *Fuel* 236, 404–427. <https://doi.org/10.1016/j.fuel.2018.08.103>.
- Jia, Y., Lu, Y., Elsworth, D., Fang, Y., Tang, J., 2018. Surface characteristics and permeability enhancement of shale fractures due to water and supercritical carbon dioxide fracturing. *J. Petrol. Sci. Eng.* 165, 284–297. <https://doi.org/10.1016/j.petrol.2018.02.018>.
- Jiang, C., Niu, B., Yin, G., Zhang, D., Yu, T., Wang, P., 2019. CT-based 3D reconstruction of the geometry and propagation of hydraulic fracturing in shale. *J. Petrol. Sci. Eng.* 179, 899–911. <https://doi.org/10.1016/j.petrol.2019.04.103>.
- Jiang, Y., Luo, Y., Lu, Y., Qin, C., Liu, H., 2016. Effects of supercritical CO₂ treatment time, pressure, and temperature on microstructure of shale. *Energy* 97, 173–181. <https://doi.org/10.1016/j.energy.2015.12.124>.
- Jiang, Y., Qin, C., Kang, Z., Zhou, J., Li, Y., Liu, H., Song, X., 2018. Experimental study of supercritical CO₂ fracturing on initiation pressure and fracture propagation in shale under different triaxial stress conditions. *J. Nat. Gas Sci. Eng.* 55, 382–394. <https://doi.org/10.1016/j.jngse.2018.04.022>.
- Johnson, E., Johnson, L., 2012. Hydraulic Fracture Water Usage in Northeast British Columbia: Locations, Volumes and Trends. *Geoscience Reports 2012. British Columbia Ministry of Energy and Mines*, pp. 41–63.
- Kan, W.H., Albino, C., da Costa, D.D., Dolman, K., Lucey, T., Tang, X., Cairney, J., Proust, G., 2018. Fracture toughness testing using photogrammetry and digital image correlation. *MethodsX* 5, 1166–1177. <https://doi.org/10.1016/j.mex.2018.09.012>.
- Kanaori, Y., Yairi, K., Ishida, T., 1991. Grain boundary microcracking of granitic rocks from the northeastern region of the Atotsugawa fault, central Japan: SEM backscattered electron images. *Eng. Geol.* 30, 221–235. [https://doi.org/10.1016/0013-7952\(91\)90044-L](https://doi.org/10.1016/0013-7952(91)90044-L).
- Kargbo, D.M., Wilhelm, R.G., Campbell, D.J., 2010. Natural gas plays in the Marcellus shale: challenges and potential opportunities. *Environ. Sci. Technol.* 44, 5679–5684. <https://doi.org/10.1021/es903811p>.
- Kizaki, A., Tanaka, H., Ohashi, K., Sakaguchi, K., Matsuki, K., 2012. Hydraulic fracturing in Inada granite and Ogino tuff with super critical carbon dioxide. In: ISRM Regional Symposium - 7th Asian Rock Mechanics Symposium. Paper Number: ISRM-ARMS7-2012-109.
- Lashgari, H.R., Sun, A., Zhang, T., Pope, G.A., Lake, L.W., 2019. Evaluation of carbon dioxide storage and miscible gas EOR in shale oil reservoirs. *Fuel* 241, 1223–1235. <https://doi.org/10.1016/j.fuel.2018.11.076>.
- Le, M.T., 2018. An assessment of the potential for the development of the shale gas industry in countries outside of north America. *Heliyon* 4 (2). <https://doi.org/10.1016/j.heliyon.2018.e00516>.
- Lei, X., Nishizawa, O., Kusunose, K., Satoh, T., 1992. Fractal structure of the hypocenter distributions and focal mechanism solutions of acoustic emission in two granites of different grain sizes. *J. Phys. Earth* 40, 617–634. <https://doi.org/10.4294/jpe.1992.40.617>.
- Lenhard, L., Andersen, S., Coimbra-Araújo, C., 2018. Energy-environmental implications of shale gas exploration in Paraná Hydrological Basin, Brazil. *Renew. Sustain. Energy Rev.* 90, 56–69. <https://doi.org/10.1016/j.rser.2018.03.042>.
- Lepillier, B., Yoshioka, K., Parisio, F., Bakker, R.R., Bruhn, D., 2020. Variational phase-field modeling of hydraulic fracture interaction with natural fractures and application to enhanced geothermal systems. *J. Geo-Phys. Res.* 125. <https://doi.org/10.1029/2020JB019856>.
- Li, B.Q., da Silva, B.G., Einstein, H., 2019. Laboratory hydraulic fracturing of granite: acoustic emission observations and interpretation. *Eng. Fract. Mech.* 209, 200–220. <https://doi.org/10.1016/j.engfracmech.2019.01.034>.
- Li, N., Zhang, S., Zou, Y., Ma, X., Zhang, Z., Li, S., Chen, M., Sun, Y., 2018. Acoustic emission response of laboratory hydraulic fracturing in layered shale. *Rock Mech. Rock Eng.* 51, 3395–3406. <https://doi.org/10.1007/s00603-018-1547-5>.
- Li, Q., Wang, Y., Wang, F., Li, Q., Kobina, F., Bai, H., Yuan, L., 2019. Effect of a modified silicone as a thickener on rheology of liquid CO₂ and its fracturing capacity. *Polymers* 11, 540. <https://doi.org/10.3390/polym11030540>.
- Li, S., Zhang, S., Ma, X., Zou, Y., Li, N., Chen, M., Cao, T., Bo, Z., 2019. Hydraulic fractures induced by water/carbon dioxide-based fluids in tight sandstones. *Rock Mech. Rock Eng.* 52, 3323–3340. <https://doi.org/10.1007/s00603-019-01777-w>.
- Li, X., Feng, Z., Han, G., Elsworth, D., Marone, C., Saffer, D., Cheon, D.S., 2016. Breakdown pressure and fracture surface morphology of hydraulic fracturing in shale with H₂O, CO₂ and N₂. *Geomechan. Geophys. Geo-Energy Geo-Resour.* 2, 63–76. <https://doi.org/10.1007/s40948-016-0022-6>.
- Liu, H., Wang, F., Zhang, J., Meng, S., Duan, Y., 2014. Fracturing with carbon dioxide: application status and development trend. *Petrol. Explor. Dev.* 41, 513–519. [https://doi.org/10.1016/S1876-3804\(14\)60060-4](https://doi.org/10.1016/S1876-3804(14)60060-4).
- Liu, L., Zhu, W., Wei, C., Elsworth, D., Wang, J., 2018. Microcrack-based geo-mechanical modeling of rock-gas interaction during supercritical CO₂ fracturing. *J. Petrol. Sci. Eng.* 164, 91–102. <https://doi.org/10.1016/j.petrol.2018.01.049>.
- Lu, T., Liu, Y., Wu, L., Wang, X., 2015. Challenges to and counter-measures for the production stabilization of tight sandstone gas reservoirs of the Sulige Gasfield, Ordos Basin. *Nat. Gas. Ind. B* 2, 323–333. <https://doi.org/10.1016/j.ngib.2015.09.005>.
- Luo, X., Wang, S., Wang, Z., Jing, Z., Lv, M., Zhai, Z., Han, T., 2015. Experimental investigation on rheological properties and friction performance of thickened CO₂ fracturing fluid. *J. Petrol. Sci. Eng.* 133, 410–420. <https://doi.org/10.1016>

- [j.petro.2015.06.033](#).
- Mahmud, H.B., Ermila, M., Bennour, Z., Mahmud, W.M., 2020. A Review of Fracturing Technologies Utilized in Shale Gas Resources. *Hydraulic Fracturing*. IntechOpen. <https://doi.org/10.5772/intechopen.92366>.
- Malik, A.R., Dashash, A.A., Driveesh, S.M., Noaman, Y.M., Soriano, E., Lopez, A., 2014. Successful implementation of CO₂ energized acid fracturing treatment in deep, tight and sour carbonate gas reservoir in Saudi Arabia that reduced fresh water consumption and enhanced well performance. In: Abu Dhabi International Petroleum Exhibition and Conference. <https://doi.org/10.2118/172620-MS>.
- Maso, G.D., Toader, R., 2002. A model for the quasi-static growth of brittle fractures: existence and approximation results. *Arch. Ration. Mech. Anal.* 162, 101–135. <https://doi.org/10.1007/s002050100187>.
- Meng, S., Yang, Q., Chen, S., Duan, Y., 2018. Fracturing with pure liquid CO₂: a case study. In: SPE Asia Pacific Oil and Gas Conference and Exhibition. <https://doi.org/10.2118/191877-18APOG-MS>.
- Middleton, R., Viswanathan, H., Currier, R., Gupta, R., 2014. CO₂ as a fracturing fluid: potential for commercial-scale shale gas production and CO₂ sequestration. *Energy Proc.* 63, 7780–7784. <https://doi.org/10.1016/j.egypro.2014.11.812>.
- Middleton, R.S., Carey, J.W., Currier, R.P., Hyman, J.D., Kang, Q., Karra, S., Jiménez-Martínez, J., Porter, M.L., Viswanathan, H.S., 2015. Shale gas and non-aqueous fracturing fluids: opportunities and challenges for supercritical CO₂. *Appl. Energy* 147, 500–509. <https://doi.org/10.1016/j.apenergy.2015.03.023>.
- Mikelić, A., Wheeler, M., Wick, T., 2015. Phase-field modeling of a fluid-driven fracture in a poroelastic medium. *Comput. Geosci.* 19, 1171–1195. <https://doi.org/10.1007/s10596-015-9532-5>.
- Mojid, M.R., Negash, B.M., Abdulelah, H., Jufar, S.R., Adewumi, B.K., 2021. A state-of-art review on waterless gas shale fracturing technologies. *J. Petrol. Sci. Eng.* 196, 108048. <https://doi.org/10.1016/j.petrol.2020.108048>.
- Mollaali, M., Ziaei-Rad, V., Shen, Y., 2019. Numerical modeling of CO₂ fracturing by the phase field approach. *J. Nat. Gas Sci. Eng.* 70, 102905. <https://doi.org/10.1016/j.jngse.2019.102905>.
- Motakabbir, K.A., Berkowitz, M.L., 1990. Isothermal compressibility of SPC/E water. *J. Phys. Chem.* 94, 8359–8362.
- Nianyin, L., Jiajie, Y., Chao, W., Suiwang, Z., Xiangke, L., Jia, K., Yuan, W., Yinhong, D., 2021. Fracturing technology with carbon dioxide: a review. *J. Petrol. Sci. Eng.* 205, 108793. <https://doi.org/10.1016/j.petrol.2021.108793>.
- Nicot, J.P., Scanlon, B., 2012. Water use for shale-gas production in Texas, US. *Environ. Sci. Technol.* 46, 3580–3586. <https://doi.org/10.1021/es204602t>.
- Nishiyama, T., Kusuda, H., 1994. Identification of pore spaces and microcracks using fluorescent resins. *Int. J. Rock Mech. Min. Sci. Geomech. Abstracts* 31, 369–375. [https://doi.org/10.1016/0148-9062\(94\)90904-0](https://doi.org/10.1016/0148-9062(94)90904-0).
- Osborn, S.G., Vengosh, A., Warner, N.R., Jackson, R.B., 2011. Methane contamination of drinking water accompanying gas-well drilling and hydraulic fracturing. In: Proceedings of the National Academy of Sciences of the United States of America, vol. 108, pp. 8172–8176. <https://doi.org/10.1073/pnas.1100682108>.
- Pan, B., 2018. Digital image correlation for surface deformation measurement: historical developments, recent advances and future goals. *Meas. Sci. Technol.* 29, 082001. <https://doi.org/10.1088/1361-6501/aac55b>.
- Pan, Y., Hui, D., Luo, P., Zhang, Y., Zhang, L., Sun, L., 2018. Influences of subcritical and supercritical CO₂ treatment on the pore structure characteristics of marine and terrestrial shales. *J. CO₂ Util.* 28, 152–167. <https://doi.org/10.1016/j.jcou.2018.09.016>.
- Pei, P., Ling, K., He, J., Liu, Z., 2015. Shale gas reservoir treatment by a CO₂-based technology. *J. Nat. Gas Sci. Eng.* 26, 1595–1606. <https://doi.org/10.1016/j.jngse.2015.03.026>.
- Pilipenko, D., Fleck, M., Emmerich, H., 2011. On numerical aspects of phase field fracture modelling. *Europ. Phys. J. Plus* 126, 100. <https://doi.org/10.1140/epjp/i2011-11100-3>.
- Pruess, K., 2008. On production behavior of enhanced geothermal systems with CO₂ as working fluid. *Energy Convers. Manag.* 49, 1446–1454. <https://doi.org/10.1016/j.enconman.2007.12.029>.
- Qu, T., Feng, Y., Wang, M., Jiang, S., 2020. Calibration of parallel bond parameters in bonded particle models via physics-informed adaptive moment optimisation. *Powder Technol.* 366, 527–536. <https://doi.org/10.1016/j.powtec.2020.02.077>.
- Randolph, J.B., Saar, M.O., 2011. Combining geothermal energy capture with geologic carbon dioxide sequestration. *Geophys. Res. Lett.* 38. <https://doi.org/10.1029/2011GL047265>.
- Ranjith, P., Zhang, C., Zhang, Z., 2019. Experimental study of fracturing behaviour in ultralow permeability formations: a comparison between CO₂ and water fracturing. *Eng. Fract. Mech.* 217, 106541. <https://doi.org/10.1016/j.engfracmech.2019.106541>.
- Roth, S.N., Léger, P., Soulaïmani, A., 2020. Strongly coupled XFEM formulation for non-planar three-dimensional simulation of hydraulic fracturing with emphasis on concrete dams. *Comput. Methods Appl. Mech. Eng.* 363, 112899. <https://doi.org/10.1016/j.cma.2020.112899>.
- Russo, M., 1978. Analysis of Fractures Utilizing the SEM. Springer US, Boston, MA, pp. 65–95. <https://doi.org/10.1007/978-1-4613-2856-8-3>.
- Solomon, S., Plattner, G.K., Knutti, R., Friedlingstein, P., 2009. Irreversible climate change due to carbon dioxide emissions. *Proc. Natl. Acad. Sci. USA* 106, 1704–1709. <https://doi.org/10.1073/pnas.0812721106>.
- Salimzadeh, S., Usui, T., Paluszny, A., Zimmerman, R.W., 2017. Finite element simulations of interactions between multiple hydraulic fractures in a poroelastic rock. *Int. J. Rock Mech. Min. Sci.* 99, 9–20. Paper Number: ARMA-2017-1044.
- Scanlon, B.R., Reedy, R.C., Nicot, J.P., 2014. Comparison of water use for hydraulic fracturing for unconventional oil and gas versus conventional oil. *Environ. Sci. Technol.* 48, 12386–12393. <https://doi.org/10.1021/es502506v>.
- Shafloot, T.A., Kim, T.W., Kovscek, A.R., 2021. Investigating fracture propagation characteristics in shale using SC-CO₂ and water with the aid of X-ray computed tomography. *J. Nat. Gas Sci. Eng.* 92, 103736. <https://doi.org/10.1016/j.jngse.2020.103736>.
- Silling, S., 2000. Reformulation of elasticity theory for discontinuities and long-range forces. *J. Mech. Phys. Solid.* 48, 175–209. [https://doi.org/10.1016/S0022-5096\(99\)00029-0](https://doi.org/10.1016/S0022-5096(99)00029-0).
- Sinal, M., Lancaster, G., 1987. Liquid co fracturing: advantages and limitations. *J. Can. Petrol. Technol.* 26. <https://doi.org/10.2118/87-05-01>.
- Skarzynski, L., Tejchman, J., 2013. Experimental investigations of fracture process using DIC in plain and reinforced concrete beams under bending. *Strain* 49, 521–543. <https://doi.org/10.1111/str.12064>.
- Soliman, M., Daal, J., East, L., 2012. Fracturing unconventional formations to enhance productivity. *J. Nat. Gas Sci. Eng.* 8, 52–67. <https://doi.org/10.1016/j.jngse.2012.01.007>.
- Song, G., Song, X., Li, G., Shi, Y., Wang, G., Ji, J., Xu, F., Song, Z., 2021. An integrated multi-objective optimization method to improve the performance of multilateral-well geothermal system. *Renew. Energy* 172, 1233–1249. <https://doi.org/10.1016/j.renene.2021.03.073>.
- Song, W., Ni, H., Tang, P., 2021. Simulation of supercritical carbon dioxide fracturing in shale gas reservoir. *J. Therm. Sci.* 30, 1444–1451. <https://doi.org/10.1007/s11630-021-1477-5>.
- Sun, B.J., Wang, J.T., Sun, W.C., Wang, Z.Y., Sun, J.S., 2019. Advance in fundamental research of supercritical CO₂ fracturing technology for unconventional natural gas reservoirs. *J. China University of Petroleum (Edition of Natural Science)* 43, 82–91 (in Chinese).
- Sun, L., Zhou, C., Jia, A., 2019. Development characteristics and orientation of tight oil and gas in China. *Petrol. Explor. Dev.* 46, 1015–1026. <https://doi.org/10.11698/PED.2019.06.01>.
- Taron, J., Elsworth, D., 2009. Thermal–hydrologic–mechanical–chemical processes in the evolution of engineered geothermal reservoirs. *Int. J. Rock Mech. Min. Sci.* 46, 855–864. <https://doi.org/10.1016/j.ijrmms.2009.01.007>.
- Tong, X., Zhang, G., Wang, Z., et al., 2018. Distribution and potential of global oil and gas resources. *Petrol. Explor. Dev.* 45 (4), 779–789. [https://doi.org/10.1016/S1876-3804\(18\)30081-8](https://doi.org/10.1016/S1876-3804(18)30081-8).
- Trickett, K., Xing, D., Enick, R., Eastoe, J., Hollamby, M., Mutch, K., Rogers, S., Heenan, R., Steytler, D., 2009. Rod-like micelles thicken CO₂. *Langmuir* 26, 83–88. <https://doi.org/10.1021/la902128g>.
- Wamock, W.E.J., Harris, P., King, D., 1985. Successful field applications of CO₂-foam fracturing fluids in the Arkansas-Louisiana-Texas Region. *J. Petrol. Technol.* 37, 80–88. <https://doi.org/10.2118/11932-PA>.
- Wang, H., Li, G., Shen, Z., 2012. A feasibility analysis on shale gas exploitation with supercritical carbon dioxide. *Energy Sources, Part A Recovery, Util. Environ. Eff.* 34, 1426–1435. <https://doi.org/10.1080/15567036.2010.529570>.
- Wang, H., Wang, M., Yang, B., Lu, Q., Zheng, Y., Zhao, H., 2018a. Numerical study of supercritical CO₂ and proppant transport in different geometrical fractures. *Greenhouse Gases Sci. Technol.* 8, 898–910. <https://doi.org/10.1002/ghg.1803>.
- Wang, H., Li, X., Sepehrmoori, K., Zheng, Y., Yan, W., 2019. Calculation of the wellbore temperature and pressure distribution during supercritical CO₂ fracturing flowback process. *Int. J. Heat Mass Tran.* 139, 10–16. <https://doi.org/10.1016/j.jijheatmasstransfer.2019.04.109>.
- Wang, H., Li, G., Zheng, Y., Kammy, S., Shen, H., 2020. Research status and prospects of supercritical CO₂ fracturing technology. *Acta Pet. Sin.* 41 (1), 116–126. <https://doi.org/10.7623/syxb202001011> (in Chinese).
- Wang, J., Liu, M., Bentley, Y., Feng, L., Zhang, C., 2018b. Water use for shale gas extraction in the sichuan basin, China. *J. Environ. Manag.* 226, 13–21. <https://doi.org/10.1016/j.jenvman.2018.08.031>.
- Wang, J., Elsworth, D., Wu, Y., Liu, J., Zhu, W., Liu, Y., 2018c. The influence of fracturing fluids on fracturing processes: a comparison between water, oil and SC-CO₂. *Rock Mech. Rock Eng.* 51, 299–313. <https://doi.org/10.1007/s00603-017-1326-8>.
- Wang, J., Sun, B., Chen, W., Xu, J., Wang, Z., 2019. Calculation model of unsteady temperature–pressure fields in wellbores and fractures of supercritical CO₂ fracturing. *Fuel* 253, 1168–1183. <https://doi.org/10.1016/j.fuel.2019.05.111>.
- Wang, L., Liang, W., 2019. Experimental study on fracture initiation and growth in coal using hydraulic fracturing with SC-CO₂ and water. *Chin. J. Rock Mech. Eng.* 2680–2689. <https://doi.org/10.13722/j.cnki.jrme.2018.0253> (in Chinese).
- Wang, L., Yao, B., Xie, H., Kneafsey, T.J., Winterfeld, P.H., Yin, X., Wu, Y.S., 2017a. Experimental investigation of injection-induced fracturing during supercritical CO₂ sequestration. *Int. J. Greenh. Gas Control* 63, 107–117. <https://doi.org/10.1016/j.jggc.2017.05.006>.
- Wang, L., Yao, B., Xie, H., Winterfeld, P.H., Kneafsey, T.J., Yin, X., Wu, Y.S., 2017b. CO₂ injection-induced fracturing in naturally fractured shale rocks. *Energy* 139, 1094–1110. <https://doi.org/10.1016/j.energy.2017.08.031>.
- Wang, M., Feng, Y., Pande, G., Zhao, T., 2018. A coupled 3-dimensional bonded discrete element and lattice Boltzmann method for fluid-solid coupling in cohesive geomaterials. *Int. J. Numer. Anal. Methods Geomech.* 42, 1405–1424. <https://doi.org/10.1002/nag.2799>.
- Wang, T., Liu, Z., Zeng, Q., Gao, Y., Zhuang, Z., 2017. XFEM modeling of hydraulic fracture in porous rocks with natural fractures. *Sci. China Phys. Mech. Astron.* 60, 84612. <https://doi.org/10.1007/s11433-017-9037-3>.
- Wang, X.Z., Wu, J.Q., Zhang, J.T., 2014. Application of CO₂ fracturing technology for terrestrial shale gas reservoirs. *Nat. Gas Ind.* 32, 64–67 (in Chinese).
- Warpinski, N., Kramm, R.C., Heinze, J.R., Waltman, C.K., 2005. Comparison of single-

- and dual-array microseismic mapping techniques in the Barnett shale. In: SPE Annual Technical Conference and Exhibition. <https://doi.org/10.2118/95568-MS>.
- Xu, D., Liu, Z., Zhuang, Z., Zeng, Q., Wang, T., 2017. Study on interaction between induced and natural fractures by extended finite element method. *Sci. China Phys. Mech. Astron.* 60, 24611. <https://doi.org/10.1007/s11433-016-0344-2>.
- Yan, H., Zhang, J., Li, M., Suo, Y., Liu, H., 2019a. New insights on supercritical CO₂ fracturing coal mass: a staged analysis method. *Greenhouse Gases Sci. Technol.* 9, 1266–1275. <https://doi.org/10.1002/ggh.1926>.
- Yan, H., Zhang, J., Zhou, N., Li, M., 2019b. Staged numerical simulations of supercritical CO₂ fracturing of coal seams based on the extended finite element method. *J. Nat. Gas Sci. Eng.* 65, 275–283. <https://doi.org/10.1016/j.jngse.2019.03.021>.
- Yang, F., Wang, X., Li, Yong, 2014. Research and application status of CO₂ fracturing fluids. *Petrochem. Industry Appl.* 15–18 (in Chinese). Link: <https://kns.cnki.net/kcms/detail/detail.aspx?FileName=NXSH201412004&DbName=CJFQ2014>.
- Yang, B., Wang, H., Wang, B., Shen, Z., Zheng, Y., Jia, Z., Yan, W., 2021a. Digital quantification of fracture in full-scale rock using micro-CT images: a fracturing experiment with N₂ and CO₂. *J. Petrol. Sci. Eng.* 196, 107682. <https://doi.org/10.1016/j.petrol.2020.107682>.
- Yang, B., Wang, H., Shen, Z., Olorode, O., Wang, B., Zheng, Y., Yan, W., Jia, Z., 2021b. Full-sample X-ray microcomputed tomography analysis of supercritical CO₂ fracturing in tight sandstone: effect of stress on fracture dynamics. *Energy Fuel.* 35, 1308–1321. <https://doi.org/10.1021/acs.energyfuels.0c03554>.
- Yang, Z.Z., Yi, L.P., Li, X.G., Chen, Y.T., Sun, J., 2018. Model for calculating the wellbore temperature and pressure during supercritical carbon dioxide fracturing in a coalbed methane well. *J. CO₂ Util.* 26, 602–611. <https://doi.org/10.1016/j.jcou.2018.06.010>.
- Zang, A., Wagner, F.C., Stanchits, S., Dresen, G., Andresen, R., Haidekker, M.A., 1998. Source analysis of acoustic emissions in aue granite cores under symmetric and asymmetric compressive loads. *Geophys. J. Int.* 135, 1113–1130. <https://doi.org/10.1046/j.1365-246X.1998.00706.x>.
- Zhang, C., Cheng, P., Ranjith, P., Lu, Y., Zhou, J., 2020. A comparative study of fracture surface roughness and flow characteristics between CO₂ and water fracturing. *J. Nat. Gas Sci. Eng.* 76, 103188. <https://doi.org/10.1016/j.jngse.2020.103188>.
- Zhang, D., Wang, P., Yang, L., 2002. The reservoir harmless fracturing-liquid CO₂ fracturing. *Oil Drilling Production Technol* 24, 47–50. <https://doi.org/10.13639/j.odpt.2002.04.021>.
- Zhang, Q., Ma, D., Liu, J., Wang, J., Li, X., Zhou, Z., 2019d. Numerical simulations of fracture propagation in jointed shale reservoirs under CO₂ fracturing. *Geofluids.* <https://doi.org/10.1155/2019/2624716>.
- Zhang, W., Wang, C., Guo, T., He, J., Zhang, L., Chen, S., Qu, Z., 2021. Study on the cracking mechanism of hydraulic and supercritical CO₂ fracturing in hot dry rock under thermal stress. *Energy* 221, 119886. <https://doi.org/10.1016/j.energy.2021.119886>.
- Zhang, X., Lu, Y., Tang, J., Zhou, Z., Liao, Y., 2017a. Experimental study on fracture initiation and propagation in shale using supercritical carbon dioxide fracturing. *Fuel* 190, 370–378. <https://doi.org/10.1016/j.fuel.2016.10.120>.
- Zhang, X., Wang, J., Gao, F., Ju, Y., 2017b. Impact of water, nitrogen and CO₂ fracturing fluids on fracturing initiation pressure and flow pattern in anisotropic shale reservoirs. *J. Nat. Gas Sci. Eng.* 45, 291–306. <https://doi.org/10.1016/j.jngse.2017.06.002>.
- Zhang, X., Zhu, W., Xu, Z., Liu, S., Wei, C., 2022. A review of experimental apparatus for supercritical CO₂ fracturing of shale. *J. Petrol. Sci. Eng.* 208, 109515. <https://doi.org/10.1016/j.petrol.2021.109515>.
- Zhang, Y., He, J., Li, F., Fan, X., Li, X., 2019a. Characteristics of fracture propagation induced by supercritical CO₂ in inter-salt-shale reservoir. *Geofluids.* <https://doi.org/10.1155/2019/7132843>.
- Zhang, Y., He, J., Li, X., Lin, C., 2019b. Experimental study on the supercritical CO₂ fracturing of shale considering anisotropic effects. *J. Petrol. Sci. Eng.* 173, 932–940. <https://doi.org/10.1016/j.petrol.2018.10.092>.
- Zhang, Z., Mao, J., Yang, X., Zhao, J., Smith, G.S., 2019c. Advances in waterless fracturing technologies for unconventional reservoirs. *Energy Sources, Part A Recovery, Util. Environ. Eff.* 41, 237–251. <https://doi.org/10.1080/15567036.2018.1514430>.
- Zhao, H., Wu, K., Huang, Z., Xu, Z., Shi, H., Wang, H., 2021. Numerical model of CO₂ fracturing in naturally fractured reservoirs. *Eng. Fract. Mech.* 244, 107548. <https://doi.org/10.1016/j.engfracmech.2021.107548>.
- Zhao, Z., Li, X., He, J., Mao, T., Zheng, B., Li, G., 2018. A laboratory investigation of fracture propagation induced by supercritical carbon dioxide fracturing in continental shale with interbeds. *J. Petrol. Sci. Eng.* 166, 739–746. <https://doi.org/10.1016/j.petrol.2018.03.066>.
- Zheng, M., Li, J., Wu, X., Wang, S., Guo, Q., Yu, J., Zheng, M., Chen, N., Yi, Q., 2018. China's conventional and unconventional natural gas resources: potential and exploration targets. *J. Natural Gas Geosci.* 3, 295–309. <https://doi.org/10.1016/j.jnggs.2018.11.007>.
- Zheng, Y., Wang, H., Yang, B., Hu, Y., Shen, Z., Wen, H., Yan, W., 2020. CFD-DEM simulation of proppant transport by supercritical CO₂ in a vertical planar fracture. *J. Nat. Gas Sci. Eng.* 84, 103647. <https://doi.org/10.1016/j.jngse.2020.103647>.
- Zhou, D., Zhang, G., Wang, Y., Xing, Y., 2018a. Experimental investigation on fracture propagation modes in supercritical carbon dioxide fracturing using acoustic emission monitoring. *Int. J. Rock Mech. Min. Sci.* 110, 111–119. <https://doi.org/10.1016/j.ijrmms.2018.07.010>.
- Zhou, D., Zhang, G., Zhao, P., Wang, Y., Xu, S., 2018b. Effects of post-instability induced by supercritical CO₂ phase change on fracture dynamic propagation. *J. Petrol. Sci. Eng.* 162, 358–366. <https://doi.org/10.1016/j.petrol.2017.12.066>.
- Zhou, D., Zhang, G., Prasad, M., Wang, P., 2019. The effects of temperature on supercritical CO₂ induced fracture: an experimental study. *Fuel* 247, 126–134. <https://doi.org/10.1016/j.fuel.2019.02.099>.
- Zhou, J., Liu, G., Jiang, Y., Xian, X., Liu, Q., Zhang, D., Tan, J., 2016. Supercritical carbon dioxide fracturing in shale and the coupled effects on the permeability of fractured shale: an experimental study. *J. Nat. Gas Sci. Eng.* 36, 369–377. <https://doi.org/10.1016/j.jngse.2016.10.005>.
- Zhou, J., Xie, S., Jiang, Y., Xian, X., Liu, Q., Lu, Z., Lyu, Q., 2018. Influence of supercritical CO₂ exposure on CH₄ and CO₂ adsorption behaviors of shale: implications for CO₂ sequestration. *Energy Fuel.* 32. <https://doi.org/10.1021/acs.energyfuels.8b00551>.
- Zhou, J., Hu, N., Xian, X., Zhou, L., Tang, J., Kang, Y., Wang, H., 2019. Supercritical CO₂ fracking for enhanced shale gas recovery and CO₂ sequestration: results, status and future challenges. *Adv. Geo Energy Res.* 3, 207–224. <https://doi.org/10.26804/ager.2019.02.10>.
- Zhou, X., Burbey, T.J., 2014. Fluid effect on hydraulic fracture propagation behavior: a comparison between water and supercritical CO₂-like fluid. *Geofluids* 14, 174–188.
- Zoback, M.D., 2010. *Reservoir Geomechanics*. Cambridge University Press, Cambridge, UK 14.
- Zou, Y., Li, N., Ma, X., Zhang, S., Li, S., 2018. Experimental study on the growth behavior of supercritical CO₂ induced fractures in a layered tight sandstone formation. *J. Nat. Gas Sci. Eng.* 49, 145–156. <https://doi.org/10.1016/j.jngse.2017.11.005>.